arXiv:hep-ph/0001265v1 25 Jan 2000

A Phenomenological Description of $\pi^-\Delta^{++}$ Photo- and Electroproduction in Nucleon Resonance Region

M. Ripani[a,1], V. Mokeev[b], M. Anghinolfi[a], M. Battaglieri[a],
G. Fedotov[d], E. Golovach[a,b], B.Ishkhanov[b,d], M. Osipenko[d],
G. Ricco[a,c], V. Sapunenko[a,b], M. Taiuti[a]

[a]Istituto Nazionale di Fisica Nucleare,
Via Dodecanneso 33, I-16146 Genova (Italy)

[b]Nuclear Physics Institute, Moscow State University,
Vorob'evy gory, 119899 Moscow, Russia

[c]Dipartimento di Fisica, Università di Genova,
Via Dodecanneso 33, I-16146, Genova, Italy

[d] Physical Faculty of Moscow State University,
Vorob'evy gory, 119899 Moscow, Russia

February 1, 2008

Abstract

The $\pi^-\Delta^{++}$ production on the nucleon by real and virtual photons is discussed as initial step in a simple model approach for the two pion photo- and electroproduction on the nucleon, with emphasis on nucleon resonance excitation which is of interest for new facilities like TJNAF. A calculation for $\pi^-\Delta^{++}$ channel in resonance excitation region is presented and compared to existing experimental data along with a discussion of physical effects that we find to be of relevance. The calculation is proposed as a starting basis for the investigation of N^* electromagnetic form factors using experimental data about two pion production by real and virtual photons.

1 Introduction.

In the total photoabsorption cross section on the proton above 400 MeV the two pion production becomes possible, as it is clearly shown by several data sets from bubble chamber real photon experiments [1, 2], as well as from exclusive electron scattering experiments [3, 4] and recent measurements with real photon beams with the DAPHNE [5, 6] and SAPHIR[6, 7] detectors. From the data one can see that the cross section for this process shows a steep rise at photon energies above threshold and then exhibits a smooth decrease,

[1]e-mail: *ripani@ge.infn.it*

although still representing a large fraction of the total hadron photoproduction at $W > 1.8$ GeV. It is well established [1, 2, 3, 4, 7] that a large contribution to this process is given by the intermediate formation of $\Delta(1236)$, $\rho(770)$ and their subsequent decay in the cascade processes

$$\gamma_{r,v}p \to \Delta^{++}\pi^- \to (p\pi^+)\pi^- \tag{1}$$

$$\gamma_{r,v}p \to \rho^0 p \to p(\pi^+\pi^-) \tag{2}$$

where indices r, v stand for real and virtual photons.

An important role in quasi two-body reactions (1),(2) is played by nucleon resonances, whose excitation is clearly seen in the total photohadronic cross section [8] as well as in exclusive channels like single pion photoproduction [9]. Many of such nucleon resonances have an appreciable branching ratio in the $\Delta\pi$ and ρN channels (see Table I) and for N^* heavier than 1.7 GeV multipion decay channels become dominant. Therefore reactions (1),(2) offer a promising opportunity to study the structure of high lying resonances composed by light u and d quarks. Moreover, quark model calculations based on the three constituent quark picture [10, 11, 12] predict more states than those found in experimental searches[13]. Some parameters for such "missing" states are shown in Table II: many of them are expected to have a strong branching ratio in the two-pion final state and weak or absent coupling to the single pion: this could be a reason for them having escaped detection in experiments with pion beams and in single pion photoproduction. An additional prediction for these unobserved states is that some of them could have sizeable electromagnetic couplings, similar to other states observed in electromagnetic production. Therefore, sizeable electromagnetic couplings and strong decays through $\Delta\pi$ or ρN channels could make poorly known states more visible as well as make some of the "missing" states appear in measurements of photo- or electroproduction of the two-pion final states. It is the aim of a wide experimental program at new facilities like TJNAF [14, 15] to investigate N^* structure and to perform a search for missing states by measuring the multipion production exclusive channels produced via electromagnetic interaction. In this paper we will focus on the particular two-pion production channel that proceeds through the $\Delta^{++}\pi^-$ intermediate state.

An important feature in the study of resonances in reactions (1),(2) is the strong contribution from non-resonant processes [2], creating a "continuum" in which resonant states are embedded. For this reason, common methods for resonance investigation such as multipole amplitude analysis [16, 17], which essentially use resonance dominance, may be not very effective for reactions (1),(2).

Different approaches to describe double pion photoproduction have been presented in a few papers[2, 18, 19, 20, 21], where models based on a variety of tree-level diagrams and a few baryon resonances have been used to calculate the two pion production. The limited number of resonances included however makes them applicable only for W lower than about 1.6 GeV; moreover non-resonant terms are not always corrected for unitarity absorption effects: actually, a very important problem in the investigation of N^* in exclusive meson production by photons is the description of non-resonant processes at $W > 1.6$ GeV, where many competitive channels open up and coupled channel calculations[22, 23] appear to be very difficult due to restricted knowledge of hadron couplings as well as to computational problems.

A phenomenological description of the interaction with open inelastic channels in the initial and final states (ISI and FSI) has been proposed first in [2]. In this approach particle absorption in the initial and final states accounts for the complexity of interactions with inelastic channels; the absorptive coefficients have been usually obtained[2, 19, 24] assuming a diffractive character of the interaction of ingoing and outgoing particles; this assumption could be justified at W values above N^* excitation region, while at $W < 2.0$ GeV other mechanisms like especially s-channel processes should contribute in ISI and FSI significantly. Moreover, the high value of the effective coupling coefficients, close to the physical limit, adopted in [2, 19], at relatively small $W \sim 1.6 - 1.7$ GeV looks somewhat artificial and not physically justified.

The need to develop a method for N^* electromagnetic form factor investigation from the experimental two-pion photo- and electroproduction data led us to the development of a phenomenological approach based on minimal model ingredients. This was accomplished parametrizing, under simple assumptions, the main two-pion photo- and electroproduction mechanisms and using experimental data to determine the corresponding parameters.

This paper is our first step in establishing such phenomenological approach: we focused our attention on the particular quasi-two-body channel (1) and set up a simple model including all known resonant states contributing to this reaction and non-resonant processes starting from a minimal set of mechanisms proposed in [2, 18]. We used existing data for the pion electromagnetic form factor to provide a description of non-resonant terms for $Q^2 > 0$, as well as data about the strong form factor in $\pi N\Delta$ vertex to take into account the particle size in hadronic vertices. Unitarity effects manifesting in the competition of many hadronic channels in non-resonant processes were taken into account effectively, implementing initial and final state interactions (ISI and FSI), in form of absorptive corrections; a new feature of our approach is that we developed a specific parametrisation of ISI and FSI mechanisms responsible for channel coupling at W $\leq$ 2 GeV, based on experimental information about hadronic scattering amplitudes in this energy region. In this regard, we examined some aspects of the N^* electromagnetic vertex dressing as related to our implementation of higher order corrections in form of ISI and FSI. We studied also the transition to the higher energy region, W $>$ 2 GeV, where the pure tree-level scheme corrected for finite size (strong form factor) and unitarity effects (ISI-FSI) fails in reproducing the experimental cross section: we found that a Regge trajectory exchange, in the particular form recently proposed[19, 25], can be a valid continuation into the higher energy region.

Our model relates N^* electromagnetic helicity couplings $A_{1/2}$, $A_{3/2}$, $C_{1/2}$ and measured cross sections for reaction (1) induced both by real and virtual photons, therefore offering a way to attempt the measurement of N^* contributions from a comparison to experimental data or a fit.

2 Helicity amplitudes and differential cross section.

The helicity representation has been chosen to describe the amplitudes for reaction (1). The differential cross section for reaction (1) induced by real or virtual photons in the

one-photon exchange approximation can be expressed as [26]:

$$\frac{d\sigma}{d\Omega_\pi^*} = \frac{1}{4K_L M_N}\left[(4\pi\alpha)\frac{1-\varepsilon}{Q^2}\frac{1}{2}L_{\mu\nu}W^{\mu\nu}\right]\frac{1}{(2\pi)^2}\frac{p_\pi^*}{4W} \tag{3}$$

$$K_L = \frac{W^2 - M_N^2}{2M_N}, \qquad \alpha = \frac{1}{137}$$

where W is CM total energy, p_π^* is the pion three momentum modulus in the CM frame, K_L is the "equivalent" photon energy, M_N is the nucleon mass, Q^2 = - q^2 where q^μ is the real-virtual photon four-momentum, ε is the photon polarization parameter, $L_{\mu\nu}$ is the leptonic tensor well-known from QED[26]. The information about hadronic production is contained in the hadronic tensor $W^{\mu\nu}$ which is a bilinear combination of hadronic currents:

$$W^{\mu\nu} = \frac{1}{2}\sum_{\lambda_p\lambda_\Delta} J_\mu^* J_\nu \tag{4}$$

related to the helicity amplitudes $\langle\lambda_\Delta\,|T|\,\lambda_\gamma\lambda_p\rangle$ according to:

$$\varepsilon_\mu(\lambda_\gamma)J^\mu(\lambda_p\lambda_\Delta) = \langle\lambda_\Delta\,|T|\,\lambda_\gamma\lambda_p\rangle \tag{5}$$

where λ_Δ, λ_p, λ_γ are helicities of Δ, proton and photon, respectively, ε^μ is the four – vector associated to the photon polarization state λ_γ and all variables are evaluated in the reaction CM frame.

Being the Δ an unstable particle, it is necessary to fold (3) on its mass distribution as follows[27]:

$$\frac{d\sigma}{d\Omega_\pi^*} = \int dM^2 \frac{1}{\pi}\frac{M_\Delta\Gamma_\Delta}{(M^2 - M_\Delta^2)^2 + M_\Delta^2\Gamma_\Delta^2}\frac{d\sigma}{d\Omega_\pi^*}(M^2) \tag{6}$$

where M^2 is the squared running invariant mass of Δ, while M_Δ, Γ_Δ are Δ mass and width, respectively.

3 The tree-level diagrams.

The mechanisms of reaction (1) were described by a minimal set of Feynman tree-level diagrams presented in Fig. 1. These diagrams can be subdivided into N^* contributions (Fig.1a) and a group of non-resonant processes, or Born terms (Fig.1b-e). The resonant part (Fig.1a) involves all relevant N^* and Δ^* excitations in s-channel. The non-resonant amplitudes correspond to the same set of mechanisms considered in [2, 18]. New features of our approach in this respect are:

1. implementation of electromagnetic vertex functions to describe the behaviour of non-resonant amplitudes at $Q^2 > 0$ and

2. implementation of a strong $\pi N\Delta$ form factor, relativistically invariant and based on the $N-N$ scattering analysis, to take into account the finite size of hadrons involved in non-resonant mechanisms.

3.1 Non-resonant processes.

The non-resonant processes are composed by the "seagull" or "contact" term (Fig. 1b) (which also naturally arises when considering the $\pi N\Delta$ vertex as described by an effective meson-baryon Lagrangian and then introducing the interaction with the electromagnetic field by the minimal coupling prescription), the t-channel pion-in-flight diagram (Fig.1c), the u-channel delta-in-flight diagram (Fig.1e) and by the s-pole nucleon term (Fig.1d)[2, 18]. To treat photon, pion and delta off-shell we introduced form factors in the corresponding vertices. Therefore Born terms (Fig.1b-e) are functions of Q^2 and Mandelstam t variables. For the vertex function evaluation we used a compilation of experimental data about electromagnetic and strong form factors [26, 28, 29, 30]; these data provide a reliable vertex function evaluation in the relevant region of Q^2 and t ($Q^2 <\sim 2\ GeV^2$, $t <\sim 2\ GeV^2$).

In momentum space, helicity amplitudes corresponding to the contact term are given by

$$f^c_{\lambda_\Delta\lambda_\gamma\lambda_p}(W,\theta) = g_c(Q^2,t)\overline{u}_\mu(p_2,\lambda_\Delta)u(p_1,\lambda_p)\varepsilon_\mu(q,\lambda_\gamma) \tag{7}$$

where W is the usual invariant CM energy, θ is the pion production angle in the hadronic CMS, p_1 and p_2 are the target nucleon and Δ-particle four momenta, q is the photon four momentum and u_μ, ε_μ and u are Rarita-Schwinger spinor-tensor for Δ-particle with λ_Δ helicity, polarisation vector for photon with λ_γ helicity and spinor for target nucleon with λ_p helicity, respectively; $g_c(Q^2,t)$ is an effective "seagull" term vertex function.

The pion-in-flight contribution in momentum representation reads:

$$f^{pif}_{\lambda_\Delta\lambda_\gamma\lambda_p}(W,\theta) =$$
$$g_\pi(Q^2,t)\frac{(2p^\mu_\pi - q^\mu)\varepsilon_\mu(q,\lambda_\gamma)}{t-m^2_\pi}\overline{u}_\nu(p_2,\lambda_\Delta)u(p_1,\lambda_p)(q^\nu - p^\nu_\pi) \tag{8}$$

where p_π is the pion momentum, m_π is the pion mass, g_π is the product of strong and electromagnetic vertex functions:

$$g_\pi(Q^2,t) = G_{\pi,em}(Q^2)G_{\pi N\Delta}(t) \tag{9}$$

The electromagnetic vertex function in this case was described by the well-known pole fit of pion form factor [26]

$$G_{\pi,em}(Q^2) = \frac{1}{\left(1+\frac{Q^2(GeV^2)}{\Lambda^2_\pi}\right)}\frac{1}{G_{\pi N\Delta}(t_{min})} \tag{10}$$

where t_{min} corresponds to pion production in hadronic CMS at zero degree angle; the factor $\frac{1}{G_{\pi N\Delta}(t_{min})}$ reflects the way of $G_{\pi em}(Q^2)$ form factor extraction from single pion electroproduction data presented in [29]. Analysis in [29] yielded $\Lambda^2_\pi = 0.462\ GeV^2$ and we used this value in calculations. However considering uncertainties in [29] as well as other data about pion electromagnetic form factor [31], we could allow for a variation of Λ^2_π cut-off parameter within $0.4 - 0.5$ GeV^2. Concerning the $\pi N\Delta$ t-dependence, we introduce as vertex function a strong form factor successfully applied in $NN \to N\Delta$ relativistic transition potentials[28, 32]

$$G_{\pi N\Delta}(t) = g_0\frac{\Lambda^2 - m^2_\pi}{\Lambda^2 - t} \tag{11}$$

The interaction constant g_0 and cut-off parameter Λ are: $g_0 = 2.1/m_\pi$ and $0.6 < \Lambda < 0.9$ GeV[28, 30]. We found that best data reproduction corresponds to $\Lambda = 0.75$ GeV. Gauge invariance implies equality of the "seagull" term coupling $g_c(Q^2, t)$ and the pion-in-flight term coupling $g_\pi(Q^2, t)$; we stress that, instead of applying specific electromagnetic and strong vertex functions to the contact term (which would imply to introduce some free parameters to be fitted), we rather fixed the *product* of them $g_c(Q^2, t)$ requiring gauge invariance.

The s-channel nucleon contribution (diagram of Fig.1d) is given by

$$f^N_{\lambda_\Delta \lambda_\gamma \lambda_p}(W, \theta) = g_N(Q^2) g_0 \frac{(2p_1^\mu + q^\mu)\varepsilon_\mu(q, \lambda_\gamma)}{s - m_N^2} \overline{u}_\nu(p_2, \lambda_\Delta) u(p_1, \lambda_p) p_\pi^\nu \tag{12}$$

where s is Mandelstam invariant $s = (q + p_1)^2$, m_N is the nucleon mass, g_N is the electromagnetic vertex function (we put the strong vertex function for s-channel equal to unity), described by the well-known dipole fit[26]:

$$g_N(Q^2) = \frac{1}{\left(1 + \frac{Q^2(GeV^2)}{0.71}\right)^2} \tag{13}$$

The last contribution to the Born terms that we considered was the Δ-in-flight (diagram of Fig.1e). The expression for such process is:

$$f^\Delta_{\lambda_\Delta \lambda_\gamma \lambda_p}(W, \theta) = 2 g_\Delta(Q^2, t) \frac{(2p_2^\mu - q^\mu)\varepsilon_\mu(q, \lambda_\gamma)}{u - m_\Delta^2} \overline{u}_\nu(p_2, \lambda_\Delta) p_\pi^\nu u(p_1, \lambda_p) \tag{14}$$

where u is Mandelstam variable corresponding to the crossed invariant momentum transfer $u = (p_1 - p_\pi)^2$; factor 2 accounts for the double electric charge of the Δ^{++} particle, while again $g_\Delta(Q^2, t)$ is the product of electromagnetic and strong vertex functions. Due to lack of information about Δ's elastic electromagnetic form factors we followed two ways to evaluate $g_\Delta(Q^2, t)$ vertex function: first, it was derived from gauge invariance of the total Born amplitude:

$$g_\Delta(Q^2, t) = \frac{g_\pi(Q^2, t) + g_N(Q^2)}{2}; \tag{15}$$

second, we used function (11) for $\pi N \Delta$ vertex, substituting mass m_π by m_Δ. In the latter choice we found the Δ-in-flight contribution to be negligible, because according to [28, 32] Λ cut-off parameter does not exceed 1.3 GeV. Of course in the second evaluation of Δ-in-flight term gauge invariance of the total Born amplitude is lost but, considering that our description of non-resonant terms aims to be phenomenological, we can assume that gauge invariance could be restored by other mechanisms not contributing significantly to the cross section. Moreover, a negligible Δ-in-flight contribution seems to be supported by the comparison with the experimental data.

3.2 The absorptive corrections.

It is well known [2] that the tree-level calculation is not able to reproduce the data extracted from experimental analysis of $\pi^- \Delta^{++}$ production. One reason is that the lowest order mechanisms for reaction (1) do not incorporate unitarity and hence interaction with other

open channels in initial and final states must be taken into account. Direct description of the unitarity effects in the initial and final states would require a simultaneous treatment of all relevant hadronic channels in a coupled channel calculation using hadronic elastic and inelastic scattering amplitudes data. The present status of the hadronic amplitudes knowledge as well as computational capabilities restrict coupled channel calculations to W lower than 1.6 GeV[22, 23], while investigation of the cross section for process (1) above 1.6 GeV is very important for N^* physics.

The description of open channels competition in non-resonance processes remains a challenging open problem of N^* structure investigation in exclusive meson photo- and electroproduction. The modern status of strong interaction theory does not allow to evaluate hadronic amplitudes and couplings from fundamental principles (i.e. QCD Lagrangian). Therefore we chose to adopt an effective treatment of unitarity effects in initial and final state; the initial and final state interactions responsible for the modification of the amplitude for reaction (1) are schematically depicted in Fig. 2. In the spirit of Vector Meson Dominance (VDM)[2], the ISI was assumed to proceed through a transition between photon and vector meson ρ. The black blobs describe all transition processes, between ρp initial and $\rho^{'}p^{'}$ intermediate states as well as between $\pi^{-'}\Delta^{++'}$ intermediate and $\pi^-\Delta^{++}$ final states.

We evaluated ISI and FSI effects in $\gamma p \to \pi^-\Delta^{++}$ reaction in the frame of a simple phenomenological recipe described in [24], where ingoing and outgoing particle interaction is described by penetration factors in the initial and final states f^j_{ISI}, f^j_{FSI}, which depend on the reaction total angular momentum j; they determine the amplitude for ρp initial state to be transformed into intermediate $\rho^{'}p^{'}$ state and the amplitude for $\pi^{-'}\Delta^{++'}$ intermediate state to be transformed into final $\pi^-\Delta^{++}$ state. According to [24, 33], the total Born amplitude $f_{\lambda_\Delta\lambda_\gamma\lambda_p}(\theta,\varphi)$ was numerically decomposed in partial waves with total angular momentum j:

$$\begin{aligned} f_{\lambda_\Delta\lambda_\gamma\lambda_p}(\theta,\varphi) &= \sum_j f^j_{\lambda\mu} d^j_{\lambda\mu}(\theta) e^{i(\lambda-\mu)\varphi} \\ f^j_{\lambda\mu} &= \int d\Omega \frac{2j+1}{4\pi} f^*_{\lambda_\Delta\lambda_\gamma\lambda_p}(\theta,\varphi) d^j_{\lambda\mu}(\theta) e^{i(\lambda-\mu)\varphi} \\ \lambda = -\lambda_\Delta, \qquad & \mu = \lambda_\gamma - \lambda_p \end{aligned} \tag{16}$$

The ISI & FSI modify the $f^j_{\lambda\mu}$ decomposition coefficients as:

$$\begin{aligned} f^{jcorr}_{\lambda\mu} &= f^j_{ISI} f^j_{\lambda\mu} f^j_{FSI} \\ \lambda = \lambda_\gamma - \lambda_p, \mu &= -\lambda_\Delta \end{aligned} \tag{17}$$

where $f^{jcorr}_{\lambda\mu}$ represent decomposition coefficients for the Born term amplitude modified by ISI & FSI. f^j_{ISI} and f^j_{FSI} factors, under the assumptions of ref. [24], can be related with S^j-matrix elements of $\pi^-\Delta^{++}$ and ρp elastic scattering amplitudes at total angular momentum j as:

$$\begin{aligned} f^j_{ISI} &= \langle \lambda_\rho \lambda_p | S^j | \lambda_\rho \lambda_p \rangle^{1/2} \\ f^j_{FSI} &= \langle \pi \lambda_\Delta | S^j | \lambda_\Delta \pi \rangle^{1/2} \end{aligned} \tag{18}$$

where λ_ρ, λ_p, λ_Δ are helicities for ρ-meson (equal to photon helicity in the VDM picture), for proton and Δ-isobar, respectively; S and T matrix elements are related as:

$$S = 1 + 2iT \tag{19}$$

The penetration coefficients f^j_{ISI} and f^j_{FSI} are unambiguously determined by $\pi^-\Delta^{++}$ and ρp elastic scattering amplitudes, therefore these amplitudes effectively describe all mechanisms (resonant and non-resonant) responsible for transitions between the initial ρp and intermediate $\rho^{'}p^{'}$ states as well as between the intermediate $\pi^{-'}\Delta^{++'}$ and final $\pi^-\Delta^{++}$ states (blobs in Fig. 2).

As mentioned in the introduction, a new feature of our approach is that, instead of using a diffractive ansatz like in the previous literature[24, 2, 19], better suited for higher energies, T-matrix elements for $\pi^-\Delta^{++}$ and ρp elastic scattering were more appropriately evaluated using data about hadronic scattering in the resonance region, as briefly described in the following paragraphs.

T-matrix elements for $\pi^-\Delta^{++}$ and ρp elastic scattering were evaluated in an isobar model [34, 35] assuming them to be a superposition of relevant N^* contributions and a smooth background as depicted in Fig. 3. The resonant part of the corresponding amplitudes was evaluated in Breit – Wigner ansatz described in details in sect. 3.3. To obtain T_{res} amplitude normalization, we considered a schematical situation, when complexity of all transitions $\rho p \to \rho^{'}p^{'}$ and $\pi^{-'}\Delta^{++'} \to \pi^-\Delta^{++}$ processes is limited to a single N^* excitation with elastic scattering as the only open channel; for this case, ingoing and outgoing particle absorption should be absent at resonant point ($W = M_{N^*}$) and the moduli of f^j_{ISI} and f^j_{FSI} coefficients should be equal to unity; from unitarity conditions and from the standard resonance phase behavior, we determined T^j_{res} amplitude normalization as $\langle f|T^j_{res}|i\rangle = i$ at $W = M_{N^*}$, therefore

$$f^j_{ISI}, f^j_{FSI} = 1 + 2i\langle f|T^j_{res}|i\rangle = -1 \tag{20}$$

This way we obtained the following relations between elastic $\pi\Delta$ and ρp scattering resonant amplitudes $\langle\pi\lambda_\Delta|T^j_{res}|\pi\lambda_\Delta\rangle$, $\langle\lambda_\rho\lambda_p|T^j_{res}|\lambda_\rho\lambda_p\rangle$ and N^* decay helicity amplitudes $\langle\pi\lambda_\Delta|T|N^*\rangle$, $\langle\lambda_\rho\lambda_p|T|N^*\rangle$:

$$\langle\pi\lambda_\Delta(\lambda_\rho\lambda_p)|T^j_{res}|\pi\lambda_\Delta(\lambda_\rho\lambda_p)\rangle =$$
$$\sum_{N^*}\left[\frac{a^{j2}_{\lambda_\Delta(\lambda_\rho\lambda_p)}}{M^2_{N^*} - W^2 - i\Gamma_{M_{N^*}}(W)M_{N^*}}\right]\left[\frac{P^c_{\pi(\rho)}}{8\pi(2j+1)W}\right] \tag{21}$$

where M_{N^*}, $\Gamma_{N^*}(W)$ are masses and W – dependent N^* decay widths, P^c_π, P^c_ρ are three – momenta moduli of pion and ρ. Summation in (21) is performed over all N^* contributing to the partial wave of total angular momentum j and presented in table III; $a^j_{\lambda_\Delta}$, $a^j_{\lambda_\rho\lambda_p}$ are decomposition coefficients of $\langle\pi\lambda_\Delta|T|N^*\rangle$ and $\langle\lambda_\rho\lambda_p|T|N^*\rangle$ N^* decay amplitudes through the states of total angular momentum j and related with N^* partial decay widths in helicity representation Γ_{λ_Δ} and $\Gamma_{\lambda_\rho\lambda_p}$ according to (31). Partial decay widths were taken from analysis [36] and transformed from LS to helicity representation.

Our approach should be somewhat modified if dressed γpN^* electromagnetic vertices are used for the resonant part of reaction (1) amplitude (sect 3.3). Indeed, in the complexity of transition mechanisms in ISI & FSI shown in Fig. 2 by black blobs, also the sequence of processes reported in Fig. 4 is effectively taken into account; that clearly represents a dressing mechanism of the γpN^* electromagnetic vertex. But for instance, N^* electromagnetic helicity amplitudes $A_{1/2}$, $A_{3/2}$ extracted from pion photoproduction data analysis[13] are usually interpreted as corresponding to dressed γpN^* verticies. Therefore, a double counting problem can arise in this case, as dressing effects of the electromagnetic

N^* vertex can be sizeable, as discussed in [37, 38]. To avoid double counting, one possibility is to exclude $\rho p \to N^* \to \rho^{'} p^{'}$ and $\pi^{-'}\Delta^{++'} \to N^* \to \pi^-\Delta^{++}$ mechanisms from ISI & FSI. To work out a phenomenological prescription for such exclusion we considered the above mentioned schematical situation, where the complexity of $\rho p \to \rho^{'} p^{'}$ and $\pi^{-'}\Delta^{++'} \to \pi^-\Delta^{++}$ transition mechanisms is restricted to single N^* excitation with only elastic scattering as open channel. Unitarity for Breit – Wigner formula can be expressed as

$$\Gamma_{tot} = \sum_i \Gamma_i, \tag{22}$$

where Γ_{tot}, Γ_i are total and partial N^* decay widths. For single N^* with only elastic open channel

$$\Gamma_{tot} = \Gamma_{el}, \tag{23}$$

where Γ_{tot}, Γ_{el} are total and elastic N^* decay width; our assumption insures that all transition mechanisms in $\rho p \to \rho^{'} p^{'}$, $\pi^{-'}\Delta^{++'} \to \pi^-\Delta^{++}$ are represented by $\rho p \to N^* \to \rho^{'} p^{'}$ and $\pi^{-'}\Delta^{++'} \to N^* \to \pi^-\Delta^{++}$ processes; therefore exclusion of N^* excitation from ISI & FSI should lead to complete absorption of ingoing and outgoing particle or to zero values for f^j_{ISI}, f^j_{FSI} penetration factors. As it follows from (19) the substitution

$$T^j_{res} \to \frac{1}{2} T^j_{res} \tag{24}$$

would correspond to vanishing f^j_{ISI}, f^j_{FSI} coefficients and, therefore, could be considered as an empirical prescription for excluding $\rho p \to N^* \to \rho^{'} p^{'}$ and $\pi^{-'}\Delta^{++'} \to N^* \to \pi^-\Delta^{++}$ mechanisms from ISI & FSI treatment.

The complete absorption of Born term amplitudes takes place only for such schematical situation (single N^* excitation with only elastic open channel) on which we based our exclusion prescription. In actual situation prescription (24) gives only partial absorption of ingoing and outgoing particles, since N^* contributing to $\pi^-\Delta^{++}$ and ρp elastic scattering have many open decay channels, while relations (21) – (24) give zero f^j_{ISI}, f^j_{FSI} coefficients only in our schematic assumption. Inelasticities ($\Gamma_{tot} \neq \Gamma_{el}$) provide instead non-zero f^j_{ISI}, f^j_{FSI} coefficients even at resonant point; N^* off-shell excitations as well as non-resonant processes also give non-zero values of f^j_{ISI} and f^j_{FSI} coefficients. We assumed that this partial absorption of Born terms can represent ISI & FSI corrections, being the contribution from $\rho p \to N^* \to \rho^{'} p^{'}$ and $\pi^{-'}\Delta^{++'} \to N^* \to \pi^-\Delta^{++}$ mechanisms excluded.

Of course our exclusion procedure (substitution (24)) should be applied only if for the resonant part of reaction (1) dressed electromagnetic $\gamma p N^*$ vertices are used. Actually, $\gamma p N^*$ vertices calculated in quark models are generally assumed to be "bare", i.e. free from higher order corrections (see for instance [11, 39]): in this case our calculation should not be affected by any double counting and therefore no exclusion procedure is necessary. The information on N^* electromagnetic form factors from the measured cross section could be extracted both with and without application of exclusion procedure: in the first case we would obtain information about dressed $\gamma p N^*$ vertices; in the second about $\gamma p N^*$ vertices without contribution from higher order corrections depicted in Fig. 4. Therefore our approach provides the flexibility of choosing one procedure or the other.

Evaluation of non-resonant part of $\pi^-\Delta^{++}$ and ρp scattering amplitude is described in more detail in [34, 35], but we want to report here the main features of our evaluation. We used data[36] on partial-wave πN elastic cross-sections with definite total angular momentum and isospin; the amplitudes for these partial waves were described by a superposition of all relevant N^* (table 3) and a particular background for each orbital momentum L and total spin S. The resonant part of πN elastic scattering amplitudes was treated in the same manner as $\pi^-\Delta^{++}$ and ρp elastic scattering processes; data[36] were used for $N^*N\pi$ couplings. Background for each LS wave was parametrized as a function of W by a simple linear dependence

$$T^j_{backgrLS} = A_{LS}W + B_{LS} \tag{25}$$

Parameters A_{LS} and B_{LS} were determined from our fit of πN elastic scattering data[34, 35]. To calculate background amplitudes for $\pi^-\Delta^{++}$ and ρp elastic scattering starting from πN elastic scattering background we used SU(3) flavour symmetry relations[34, 35]. The fit results for πN partial elastic scattering cross – section are shown in Fig. 5. Dotted curves represent resonant contributions, dashed lines are background contributions, while solid lines correspond to complete amplitudes. As follows from Fig. 5, in N^* excitation region nucleon resonances provide the main contribution in πN elastic amplitudes, therefore also in penetration coefficients (17). This contribution was completely neglected in previous evaluations [2, 19]. Hence, implementation of s – channel N^* excitation amplitude performed in our approach is particularly important for ISI & FSI treatment in N^* excitation region. For W above 2.0 GeV the contribution of resonant part in πN elastic scattering partial waves (Fig. 5) falls down drastically and non – resonant processes provide the main contribution for most partial waves. Therefore a diffractive approximation for ISI and FSI absorptive corrections [24, 2, 19] could be justified above N^* excitation region.

To check the reliability of our approach to evaluate ISI and FSI absorptive factors, we also performed calculations of such effects implementing $\pi^-\Delta^{++}$ and ρp elastic scattering amplitudes directly provided by the authors of analysis [40, 41], based on a global unitary fit of πN scattering T-matrix. The gross features of ISI and FSI absorptive factors as obtained from these two procedures are in reasonable coincidence [34, 35]. It is also worth to note that using the above mentioned description of Born terms, together with our ISI-FSI description, non-resonant processes in our approach do not have any free parameters to be determined from reaction (1).

Actually, our approach for ISI & FSI treatment is mostly phenomenological and our assumptions can be mainly justified by comparison with experimental data (we will discuss it in more detail in the next sections): pure Born terms give rise to a cross section that does not reproduce real photon data at high W by a large factor, while absorption-corrected calculations are able to give a good account of data up to W around 2 GeV. Implementation of pion Regge trajectory exchange according to prescription [25] in Born terms allows to obtain a satisfactory data description up to W=3 GeV as discussed in section 4.

Assuming vector dominance as main mechanism responsible for Q^2 evolution of coupling with other hadronic channels in the initial state we obtained the following expression for the f^j_{ISI} absorptive factor Q^2 dependence:

$$f^j_{ISI}(Q^2) = \frac{\Lambda^2_\pi f^j_{ISI}(Q^2=0) + Q^2}{\Lambda^2_\pi + Q^2} \tag{26}$$

where $\Lambda_\pi^2 = 0.46$ GeV^2[29].

3.3 Resonance contribution.

A simple Breit-Wigner ansatz was chosen to describe the coherent superposition of all relevant N^*, Δ^* resonant amplitudes[27] (see Table I, Fig. 1a).

$$\langle \lambda_\Delta \left| T_{res} \right| \lambda_\gamma \lambda_p \rangle = \sum_{N^*,\Delta^*} \langle \pi \lambda_\Delta \left| T_{dec} \right| \lambda_R \rangle \frac{1}{M_{res}^2 - W^2 - i\Gamma_{res}(W) M_{res}} \langle \lambda_R \left| T_{em} \right| \lambda_\gamma \lambda_p \rangle \quad (27)$$

where M_{res}, Γ_{res} are resonance mass and energy-dependent total width and $\langle \lambda_R \left| T_{em} \right| \lambda_\gamma \lambda_p \rangle$, $\langle \pi \lambda_\Delta \left| T_{dec} \right| \lambda_R \rangle$ are electromagnetic production and strong decay amplitudes of N^* with helicity $\lambda_R = \lambda_\gamma - \lambda_p$, respectively. The N^* off-shell effects were taken into account by the Breit-Wigner propagator in (23) as well as by the W-dependence of resonance width and strong decay amplitudes.

Following a phenomenological approach we related $\langle \lambda_R \left| T_{em} \right| \lambda_\gamma \lambda_p \rangle$ and $\langle \pi \lambda_\Delta \left| T_{dec} \right| \lambda_R \rangle$ amplitudes with observables extracted from experimental data analysis. Electromagnetic N^* amplitudes $\langle \lambda_R \left| T_{em} \right| \lambda_\gamma \lambda_p \rangle$ were expressed in terms of commonly used helicity couplings $A_{1/2}$, $A_{3/2}$ and $C_{1/2}$[13, 42]. Comparison of the cross section for only one isolated N^* state calculated according to (3)-(6) with Breit-Wigner formula gives:

$$\begin{aligned} \langle \lambda_R \left| T_{em} \right| \lambda_\gamma \lambda_p \rangle &= \frac{W}{M_{res}} \sqrt{\frac{8 M_N M_{res} p^*_{\gamma_R}}{4\pi\alpha}} \sqrt{\frac{p^*_{\gamma_R}}{p^*_\gamma}}\, A_{1/2,3/2}(Q^2);\ |\lambda_\gamma - \lambda_p| = \frac{1}{2}, \frac{3}{2} \\ &\quad - for\ transverse\ photons \\ \langle \lambda_R \left| T_{em} \right| \lambda_\gamma \lambda_p \rangle &= \frac{W}{M_{res}} \sqrt{\frac{8 M_N M_{res} p^*_{\gamma_R}}{4\pi\alpha}} \sqrt{\frac{p^*_{\gamma_R}}{p^*_\gamma}}\, C_{1/2}(Q^2) \\ &\quad - for\ longitudinal\ photons \end{aligned} \quad (28)$$

where $p^*_{\gamma_R}$ and p^*_γ are photon three-momentum moduli in the CM frame at resonance point ($W = M_{res}$) and at running W, respectively. Couplings $A_{1/2}(Q^2)$, $A_{3/2}(Q^2)$, $C_{1/2}(Q^2)$ completely describe N^* electromagnetic excitation and their values, calculated in a model or taken from some experimental analysis, can be used to calculate the resonant part of cross section for reaction (1). On the other hand, considering these couplings as parameters our approach could be used to attempt their extraction from a fit of the measured cross section.

The N^* strong decay amplitudes $\langle \pi \lambda_\Delta \left| T_{dec} \right| \lambda_R \rangle$ were parametrised through the projection on the set of states with definite total angular momentum j:

$$\langle \pi : \lambda_\Delta \left| T_{dec} \right| \lambda_R \rangle = a^j_{\lambda_\Delta} d^j_{\lambda_R - \lambda_\Delta}(\theta^*) \sqrt{\frac{p^*_{\pi_R}}{p^*_\pi}} e^{-\lambda_\Delta i\varphi} \quad (29)$$

where $a^j_{\lambda_\Delta}$ is the decomposition coefficient, that does not depend on the resonance helicity state due to rotational invariance, θ^* is the CM pion emission angle, $p^*_{\pi_R}$ and p^*_π are CM pion three-momentum moduli at resonance and running W, respectively. We then related the $a^j_{\lambda_\Delta}$ parameters with the partial decay widths $\sqrt{\Gamma_{ls}}$ of $N^* \to \Delta^{++} + \pi^-$ in LS-representation extracted in analysis [36].

This way we obtained the decay amplitudes at the resonance point. General requirements for the amplitude threshold behaviour[43] as well as data analysis of single-pion production by photon and pion beams[9, 44] suggest the introduction of a W dependence of N^* decay amplitudes in (27). Assuming as usually that barrier penetration effects provide a good description of W- evolution in $\langle \pi\Delta(ls)|T_{dec}|R\rangle$ decay amplitudes and using the parametrization from [36] we arrived to:

$$\langle \pi\Delta : (ls)\,|T_{dec}|\,R\rangle(W) = \\ \langle \pi\Delta : (ls)\,|T_{dec}|\,R\rangle(M_{res}) \left[\frac{M_{res}}{W}\frac{J_l^2(p^*_{\pi_R}R)+N_l^2(p^*_{\pi_R}R)}{J_l^2(p^*_{\pi}R)+N_l^2(p^*_{\pi}R)}\right]^{1/2} \tag{30}$$

where J_l, N_l are Bessel's and Neumann's functions and the factor in square brackets in (30) appears from barrier penetration ratio[45] for a particle emitted with relative orbital momentum l, while R is an interaction radius whose value was set to 1 fm. The decay amplitude (30) was then transformed into the helicity representation $\langle \lambda_\Delta\,|T_{dec}|\,\lambda_R\rangle$ and using the relationship between two-body decay amplitude and width Γ_{λ_Δ} we obtained:

$$\begin{aligned} \left|a^j_{\lambda_\Delta}\right| &= \frac{2\sqrt{2\pi}M_{res}\sqrt{2j+1}\sqrt{\Gamma_{\lambda_\Delta}}}{\sqrt{\langle p_\pi\rangle}} \\ \langle p_\pi\rangle &= \int_{(m_\pi+m_N)^2}^{(W-m_\pi)^2} dM^2 \frac{1}{\pi}\frac{M_\Delta\Gamma_\Delta}{(M^2-M_\Delta^2)^2+M_\Delta^2\Gamma_\Delta^2}p_\pi(M^2) \\ p_\pi(M^2) &= \frac{W^2+m_\pi^2-M^2}{2W} \end{aligned} \tag{31}$$

where the integration over running Δ mass squared M^2 takes into account the unstable character of Δ particle and the quantity $\sqrt{\Gamma_{\lambda_\Delta}}$ contains the above mentioned W evolution according to (30).

The total N^* decay width ($\Gamma_{res}(W)$ in (27)) was assumed to be a sum over all partial widths presented in [36]. The W evolution of each partial width $\Gamma_i(W)$ was evaluated again based on a barrier penetration ansatz:

$$\Gamma_i(W) = \Gamma_i(W=M_{res})\frac{M_{res}}{W}\frac{J_l^2(p^*_{\pi_R}R)+N_l^2(p^*_{\pi_R}R)}{J_l^2(p^*_{\pi}R)+N_l^2(p^*_{\pi}R)} \tag{32}$$

where p^*_π and $p^*_{\pi_R}$ are three-momenta moduli of meson at running W and at resonance point respectively.

The total amplitude of $\gamma p \to \Delta^{++}\pi^-$ process was then evaluated as a coherent superposition of resonant and total Born amplitude $f^{B^{corr}}_{\lambda_\gamma\lambda_p\lambda_\Delta}$, corrected for ingoing and outgoing channel absorption:

$$\langle \pi\lambda_\Delta\,|T|\,\lambda_\gamma\lambda_p\rangle = \langle \pi\lambda_\Delta\,|T_{res}|\,\lambda_\gamma\lambda_p\rangle + f^{B^{corr}}_{\lambda_\gamma\lambda_p\lambda_\Delta} \tag{33}$$

4 Results and discussion.

Using the above described approach we performed a cross section calculation for reaction (1). The resonances included in the evaluation are listed in Table I. The relative contribution of a particular N^* in the cross section can be described by the factor of merit

$\sqrt{\Gamma_{\gamma p}\Gamma_{\Delta\pi}}/\Gamma_{tot}$[1] also reported in Table I. All three- and four-star resonances[13] with $\sqrt{\Gamma_{\gamma p}\Gamma_{\Delta\pi}}/\Gamma_{tot} > 0.1\%$ were included. As follows from Table I, $F_{15}(1680)$, $D_{33}(1700)$ and $F_{37}(1950)$ resonances give maximum contribution and reaction (1) presents a promising opportunity for investigation of their structure.

As mentioned in sect. 3.1, we adopted two ways for Δ-in-flight term evaluation: a) from gauge invariance requirements; b) neglecting this term due to proximity of Δ mass and Λ cut-off parameter.

Neglecting Δ-in-flight term we obtained a better data description at high W value and pion emission angles. The results are presented in Fig. 6 by solid lines. The data are reasonably reproduced in the overall W region. A remarkable point is that our calculations predict cross sections at $\theta^*_\pi > 120^0$ and $W > 1.8$ GeV lower than 1.2 μb/sr; such strong cross section suppression namely results from absorption in the initial and final states due to interactions with open hadronic channels. For W = 1.62 GeV the calculated cross sections are a bit below the data points; this discrepancy could be ascribed to simultaneous uncertainties in the cut-off parameter appearing in the strong vertex function used for the Born terms, in the $\pi^-\Delta^{++} \to \pi^-\Delta^{++}$, $\rho^0 p \to \rho^0 p$ elastic amplitudes appearing in the absorption parameterisation, as well as to uncertainties in some s-channel N^* electromagnetic and strong parameters. The Born term contribution in angular distributions for reaction (1) is shown by dashed lines in Fig. 6, therefore the maximum N^* contribution takes place for CM pion emission angle above 90^0. The evaluation of angular distributions performed by varying N^* strong decay couplings inside uncertainties of analysis [36] demonstrated that the cross section variation does not exceed a few percent, being negligible compared with data uncertainties: therefore, our approach for the non-resonant background appears to be quite stable with respect to N^* strong decay parameter variation; this is an important feature for the extraction of N^* electromagnetic form factors from measured cross sections.

The comparison between the calculated total cross section for reaction (1) with recent SAPHIR data[7] as well as with old ABBHHM Collaboration data[1] is presented in Fig. 7. Decomposition of the total cross-section for reaction (1) in resonant, non-resonant processes and interference terms is also shown in Fig. 7. The maximum contribution of N^* (at level $20 - 30\%$) is found at $W < 1.6$ GeV and decreases as W increases. The region $W < 1.6$ GeV also corresponds to maximum contribution of interference effects in coincidence with results presented in [20, 21].

To demonstrate the effects of $\pi N\Delta$ form factor implementation as well as ISI and FSI absorptive corrections, we also reported in Fig. 8 calculation results assuming: a) $\pi N\Delta$ form factor equal to unity and absence of absorptive corrections (dashed line in Fig. 8); b) $\pi N\Delta$ form factor from [32] and absence of absorptive corrections (dotted line in Fig. 8); c) complete model (solid line). Calculation a) is not able to reproduce data at all: at $W > 1.6$ GeV the difference between calculated and measured cross-section marks the complete failure of the pure Born terms calculation. Implementation of $\pi N\Delta$ strong form factor turns out to be very important (dotted line of Fig. 8): we stress that such strong vertex function was taken from N – N scattering analysis without further tuning and assumed to be appropriate to describe the $\pi N\Delta$ vertex in the t-channel pion exchange diagram, while for the contact term which is of similar magnitude as the pion exchange, we

[1] Proportional to peak amplitude for Breit-Wigner curve.

used gauge invariance as guidance for the vertex functions evaluation. However without initial and final state absorptive corrections it is not possible to reproduce data at W above 1.7 GeV. On the other hand, even neglecting ISI and FSI effects our approach is able to describe reasonably the data at $W < 1.6$ GeV. Implementation of ISI and FSI absorptive correction factors provides a reasonable agreement between measured and calculated cross sections for W below 1.8 GeV, while for W above 1.9 GeV calculated cross sections are systematically higher than data. The reason for such deviation could be connected to the description of $\pi\Delta$, ρp elastic scattering amplitudes in ISI-FSI: this aspect could be improved by adding contributions from isobar states with higher mass and spin; another explanation could be that for W above 1.9 GeV we may start to observe a transition from the corrected Born terms picture to other processes, as those discussed in [19, 25]; in this case, the framework for non-resonant reaction mechanisms in $\gamma p \to \pi^- \Delta^{++}$ reaction should be modified at W above 1.9 GeV. We discuss these aspects in the next paragraph, to examine the limits of applicability of our meson-baryon approach and study how to continue the description of reaction (1) in the higher energy region.

Following the recipe of [19, 25], we replaced the pion exchange amplitude in Born term (Fig. 1c) by a pion Regge trajectory exchange. The results are presented in Fig. 9 (dotted line) and compared with the non-reggeized pion exchange (solid line). Regge trajectory exchange implementation provides a better data description at high W values. However, even in this case the calculated cross section appears to be systematically higher than the data. The possible reason could be the need to modify also the contact term in the way proposed in [25], thereby restoring gauge invariance. We found that such contact term modification led to a sizeable cross section reduction at W below 1.6 GeV, where descriptions in the frame of pion and Regge trajectory exchange have to coincide. To provide this coincidence we had to require $N\Delta$ – (pion Regge trajectory) effective coupling to be a factor 1.2 higher than $\pi N\Delta$ coupling. The cross section calculated under this assumption is shown in Fig. 9 with a dashed line and reproduces reasonably the data up to 2.5 GeV. As mentioned above, non – resonant part for $\pi^- \Delta^{++}$ and ρp elastic scattering amplitudes in ISI-FSI was estimated from πN scattering partial wave data fit[36], containing data up to W = 2.1 GeV. This is the main reason to restrict our calculation to W = 2.5 GeV (3 GeV photon energy in lab. frame). Implementation of any data on $\pi^- \Delta^{++}$ and ρp elastic scattering amplitudes above 2 GeV would allow a model extension toward higher W.

To investigate the influence of $\gamma p N^*$ vertex dressing on our cross section, we reported in Fig. 10 the calculations with N^* electromagnetic helicity amplitudes taken from PDG[13] and from quark models[10, 12, 39]. In the PDG case, we assumed the effects of $\gamma p N^*$ vertex dressing at level of meson – baryon degrees of freedom to be included in the numbers quoted, while in the quark models case we assumed such effects not to be accounted for ("bare" $\gamma p N^*$ vertices). Therefore, using the PDG amplitudes we applied our prescription (24) for removal of N^* dressing in ISI-FSI, while in cross section calculations with $\gamma p N^*$ vertices from quark models we kept N^* excitation terms in ISI & FSI mechanisms with no modification. In principle, one would expect these two results approximately to coincide, assuming that the same dressing effects are introduced one way or another. Our results show that this is not the case, being the cross section calculated using the "dressed" PDG values systematically higher than the quark model results; moreover, if we removed completely the N^* from the ISI-FSI description, the discrepancy would be even bigger; we

also found that the difference between the two quark model cross sections is significantly smaller than the deviation between quark model and PDG results. Actually, the difference between the cross section evaluated with "bare" and "dressed" vertices could be due to specific approximations of quark model approaches[10, 12, 39]; or it could be an indication that additional dressing effects are present in the experimentally extracted photocouplings from [13]. This difference does not exceed 30 %, with a maximum at W between 1.5 – 1.7 GeV. This W range actually corresponds to maximum N^* contribution. The discrepancy appears to be negligible at W above 2.0 GeV and below 1.4 GeV, where N^* contributions are less pronunced.

To see the influence of particular dressing effects – N^* excitation in $\pi^-\Delta^{++}$ and ρp elastic scattering processes shown in Fig. 4c – we performed calculations using "dressed" N^* electromagnetic vertices[13], but keeping the N^* excitation in ISI & FSI mechanisms for Born terms. The results are shown in Fig. 10 by dotted line; of course in this case some double counting of the N^* electromagnetic vertex dressing takes place, but surprisingly the cross section seems to be in better agreement with the "bare" quark model results. In any case, the difference between solid and dotted curves could be considered as estimation of this particular $\gamma p N^*$ vertex dressing contribution in the cross section. This contribution is lower than 20 % and vanishes at W above 2.0 GeV, where N^* excitation is negligible.

To extract N^* helicity amplitudes for $Q^2 > 0$ it is important to have a good description of the Q^2 dependence for non-resonant processes. We checked this point by comparing the total cross section for reaction (1) calculated in our approach with data reported in [4]. For the resonant part we used results from a Single Quark Transition Model (SQTM) fit[46] about the Q^2 evolution of N^* photocouplings. The comparison between data[4] and our calculations is presented in Fig. 11 where dashed lines correspond to the contribution of non – resonant processes only, while the complete evaluation with N^* included is shown by solid lines. Considering this comparison, two important points must be stressed: first, bins for experimental data[4], both in W and Q^2 were very wide, implying a strong cross section averaging over the measured kinematical range; second, experimental data about high-lying N^* photocouplings are rather scarce and do not allow to check the validity of SQTM predictions. However, our approach reproduces the measured cross-section for W in the 1.3-1.5 GeV and in the 1.5-1.7 GeV interval; for W in the 1.7-2.0 GeV bin our calculated cross-section is higher than the measurements; the reasons for such deviation could be namely the poor knowledge of the N^* contributions or the kinematical average effects, as well as the above mentioned limitations in the treatment of Born terms absorption in the higher W region. New high precision data upcoming from new facilities like TJNAF are therefore definitely needed for a better understanding of the Q^2 behaviour of N^* electromagnetic form factors. An important prediction of our evaluations is a strong N^* contribution in the W = 1.5 – 1.7 GeV interval, representing over 60 % of cross section at $Q^2 \sim 1.0$ GeV^2. Therefore the two pion exclusive channel seems to present a promising opportunity for N^* structure investigation by photons with high virtuality.

To investigate N^* electromagnetic vertex dressing effects on the cross section at $Q^2 > 0$, we performed the calculation with N^* electromagnetic form factors taken from different approaches[12, 39, 46]. Form factors in approach[46] were determined from exclusive single pion production data analysis, imposing symmetry relations between form factors of N^*'s belonging to a particular SU(6) multiplet: therefore they can be assumed to represent "dressed" vertices. Instead, quark models [12, 39] should not contain higher

order corrections and we considered their results as representing "bare" vertices. Again we expected to have approximate coincidence of results obtained using these different ingredients. Actually in this case, according to Fig. 12, the difference between cross sections calculated with the two "bare" vertices [12] and [39] is higher than the difference between results obtained using form factors from [46] and quark models results. Also in this case we calculated the cross section using "dressed" vertices from [46], with and without prescription (24) for N^* removal in ISI-FSI (solid and dotted curve in Fig. 12, respectively); in the latter case the result is supposed to be affected by double counting, but the difference can give an indication of the extent of dressing introduced by our effective unitarity implementation; as shown in Fig. 12, such effect appears to be negligible, thereby indicating that, for the $Q^2 > 0$ evolution in our framework, quark model theoretical uncertainties could be more important than dressing effects. Therefore, comparison of cross sections calculated in our approach with forthcoming precise experimental data at $Q^2 > 0$ can provide a promising opportunity to select between model approaches for N^* structure description in non – perturbative QCD region.

As mentioned above, we also compared the cross section calculated using "dressed" N^* form factors[46] with/without implementation of N^* excitation in ISI & FSI mechanisms (dotted and solid lines in Fig. 12). The contribution of this particular dressing mechanism is negligible for W$\sim$ 1.4 and 1.85 GeV and vanishes at $Q^2 > 0.5$ GeV^2 for W $\sim$ 1.6 GeV. There are actually reasons for such behaviour: a) the relative contribution of non – resonant processes drastically falls down as Q^2 increases (from more than 80 % at the photon point to lower than 50 % at Q^2 above 1 GeV^2; b) the ISI effects also go down as Q^2 increases due to suppression of transitions between photon and vector meson.

5 Conclusions.

We have extensively studied a phenomenological model for the two pion photo- and electroproduction through the intermediate $\Delta^{++}\pi^-$ channel, as part of a broader effort in establishing a basis for analysis and interpretation of the upcoming data from TJNAF[14, 15], where this as well as other exclusive electromagnetic production channels will be studied with unprecedented accuracy.

Our calculation included a minimal set of Born amplitudes, with appropriate absorptive corrections to effectively take into account interaction with open channels in the initial and final states, plus a large number of nucleon resonances that, according to the existing data, are thought to give a sizeable contribution to the cross section.

A strong form factor for $\pi N\Delta$ vertex was introduced according to NN scattering experiments. Data about pion and proton electromagnetic form factors were also used to evaluate the pion-in-flight term and the s-channel nucleon pole term, respectively, for $Q^2 > 0$, while the Q^2 behaviour of the contact term was obtained imposing gauge invariance; the delta-in-flight term was calculated both from gauge invariance and using a $\pi N\Delta$ vertex determined from NN scattering analysis. Strong and electromagnetic N^* couplings were related with experimental observables: electromagnetic helicity couplings $A_{1/2}$, $A_{3/2}$, $C_{1/2}$ and partial hadronic decay widths Γ_{ls}.

We found that strong absorptive corrections were essential to reproduce experimental data for CM pion emission angle above 30^0 at W above 1.6 GeV. We developed a specific

approach for ISI and FSI absorptive corrections, relating absorptive factors in ingoing and outgoing channels with $\pi^-\Delta^{++}$ and ρp elastic scattering amplitudes. These elastic strong amplitudes were evaluated in a simple isobaric model, so that our approach did not have any free parameters to be determined from reaction (1). Any other approach for $\pi^-\Delta^{++}$ and ρp elastic amplitude evaluation can be easily implemented in our calculation. Reasonable reproduction of pion angular distributions in the photon point as well as good agreement between measured and calculated total cross sections for $Q^2 > 0$ demonstrate the ability of our approach to reproduce the main features of $\pi^-\Delta^{++}$ production by real and virtual photons in the resonance region. Moreover the proposed method for ISI and FSI description can be considered as a reasonable phenomenological way to describe non-resonant processes in electromagnetic meson production for $W > 1.6$ GeV, where the competition of many open hadronic channels makes a rigorous background evaluation very difficult. Our unitarity corrections effectively introduce a dressing of the resonance amplitudes; therefore we elaborated an empirical prescription to remove the dressing from ISI-FSI when using experimental resonance photocouplings, assumed to be already "dressed"; we also performed calculations without this prescription when using resonance amplitudes from quark models, asssumed to be "bare". In the real photon case, we found that the calculations performed with two different quark models show a good agreement, while the results obtained using the experimental PDG amplitudes show a systematic disagreement with the previous ones; the reason is unclear and could be connected to other dressing effects than N^* excitation in $\rho p \to \rho^{'} p^{'}\ \pi^{-'}\Delta^{++'} \to \pi^-\Delta^{++}$ transitions as well as to quark model uncertainties and also to model-dependence in the experimental resonance amplitude extraction. We performed the same analysis for the virtual photon cross section, but in this case we found a disagreement between the two quark models adopted, while the calculation based on resonance amplitudes extracted from an analysis of experimental data showed less sensitivity to our "dressing" effects: the quark models discrepancies appeared to be more important, leading us to believe that in the virtual photon case the sensitivity to different quark model ingredients could be more pronunced, although the reason for the different behaviour of real and virtual photon is not evident.

The calculation presented could serve as a first basis for interpreting the data coming from new facilities like Jefferson Lab and moreover, allowing the resonance parameters to vary, it could be the starting point of a fitting procedure with the goal of investigating electromagnetic form factors for high mass N^*'s ($M_{res} > 1.5$ GeV), as well as for attempting to discover new states. The model presented is currently being used as a foundation in our development of a full three-body final state description for the two-pion production off the nucleon by real and virtual photons[15, 47].

Acknowledgements

Our special thanks to Dr. V. Burkert from Jefferson Laboratory, for continuos interest, useful discussions and support. Particular thanks to Prof. S. Dytman from the University of Pittsburgh, for kindly providing the elastic hadronic amplitudes from his global fit and to Prof. M. Giannini from the University of Genova, Italy, for kindly providing the N^* electromagnetic transition amplitudes from his quark model. We also want to thank Prof. N.C. Mukhopadhyay from Rensselaer Polytechnic Institute, for useful discussions and suggestions.

References

[1] Cambridge Bubble Chamber Group, Phys. Rev. 155, 1477(1967); ABBHHM Collaboration, Phys. Rev. 175, 1669 (1968).

[2] D. Luke and P. Soding, Springer Tracts in Mod. Phys. 59 (1971).

[3] I. Damman et al., Nucl. Phys. B54, 355(1973).

[4] K. Wacker et al., Nucl. Phys. B144, 269(1978).

[5] A. Braghieri et al., Phys.Lett. B363, 46-50(1995).

[6] B. Krusche, in Proceedings of the "Joint ECT*/JLAB Workshop on N* Physics and Nonperturbative QCD", Trento, Italy, May 18-29, 1998, ed. by S. Simula, B. Saghai, N.C. Mukhopadhyay, V.D. Burkert, Few Body Systems, Suppl. 11, 1999.

[7] F.J. Klein, Bonn University thesis BONN-IR-96-08.

[8] T.A Armstrong et al., Phys. Rev. D5, 1640 (1972); T.A. Armstrong et al., Nucl. Phys. B41, 445 (1972).

[9] R. Walker, Phys. Rev. 182, 1729(1969); R.G. Moorhouse et al., Phys. Rev. D9, 1(1974).

[10] R. Koniuk, N. Isgur, Phys. Rev. Lett. 44, 845(1980); R. Koniuk, N. Isgur, Phys. Rev. D21, 1868(1980); R. Koniuk, Nucl. Phys. B195, 452(1982).

[11] S. Capstick, W. Roberts, Phys. Rev. D49, 4570(1994).

[12] R.Bijker, F. Iachello, A. Leviatan, Phys. Rev. C54, 1935(1996).

[13] Particle Data Group, Phys. Rev. D54, 1(1996).

[14] V.D. Burkert, in Proceedings of the "Joint ECT*/JLAB Workshop on N* Physics and Nonperturbative QCD", Trento, Italy, May 18-29, 1998, ed. by S. Simula, B. Saghai, N.C. Mukhopadhyay, V.D. Burkert, Few Body Systems, Suppl. 11, 1999.

[15] M. Ripani, in Proceedings of the "Joint ECT*/JLAB Workshop on N* Physics and Nonperturbative QCD", Trento, Italy, May 18-29, 1998, ed. by S. Simula, B. Saghai, N.C. Mukhopadhyay, V.D. Burkert, Few Body Systems, Suppl. 11, 1999.

[16] F.A. Berens, A. Donnachie, Nucl. Phys. B84, 342(1975).

[17] R.A. Arndt, I.I. Strakovsky, R.L. Workman, Phys. Rev. C53, 430(1996).

[18] A. Bartl, W. Majerotto, D. Schildknecht, Nuovo Cimento 12A, 703(1972).

[19] L.Y. Murphy, J.M. Laget, DAPNIA-SPHN-96-10, Mar. 1996.

[20] J.A. Gomez-Tejedor and E. Oset, Nucl.Phys. A571, 667(1994); J.A. Gomez-Tejedor and E. Oset, Nucl.Phys. A600(1996).

[21] K. Ochi, M. Hirata, T. Takaki, Phys. Rev., C56, 1472(1997).

[22] S. Nozawa, B. Blankleider, T.-S.H Lee, Nucl. Phys. A513, 459(1990).

[23] Surya, F. Gross, Preprint CEBAF-TH-95-04&WM-95-101.

[24] K.Gottfried and J.D.Jackson, Nuovo Cimento. 34, 736(1964).

[25] M. Guidal, J.-M. Laget, M. Vanderhaeghen, Phys. Lett., B400, 6 (1997).

[26] E. Amaldi, S. Fubini, G. Furlan, Pion Electroproduction. Springer Tracts in Modern Physics, 83(1989).

[27] M. Pilkuhn, Relativistic Particle Physics. Springer Verlag (1979).

[28] R. Machleidt in Advances in Nuclear Physics v.19 (1979).

[29] C.J. Bebek et al., Phys. Rev. D17 1693(1978).

[30] L. Y. Glozman, et al., piN Newslett. 14, 99 (1998)

[31] P. Brauel, T.Canzler, e. a., Phys. Lett., 69B, 253 (1977).

[32] R. Machleidt, K Holinde, Ch. Elster, Phys. Rep. 149, 1(1987).

[33] M.Jacob and G.C Wick, Ann. of Phys. 7, 404(1959).

[34] M. Battaglieri et al., Bull. of Moscow State University (accepted for publication)

[35] M. Anghinolfi et al., Physics of Atomic Nuclei 63(2000) N1.

[36] D.M.Manley, E.M.Salesky, Phys. Rev. D45, 4002(1992).

[37] J.H. Koch, E. Moniz, Ann. Phys. (N.Y.) 154, 99(1984)

[38] T. S. H. Lee in Proceedings of the "Joint ECT*/JLAB Workshop on N* Physics and Nonperturbative QCD", Trento, Italy, May 18-29, 1998, ed. by S. Simula, B. Saghai, N.C. Mukhopadhyay, V.D. Burkert, Few Body Systems, Suppl. 11, 1999, p157.

[39] M. Ferraris et al., Phys. Lett. B364, 231 (1995); M. Aiello et al., J. Phys. G: Nucl. Part. Phys. 24, 753 (1998); M. M. Giannini, E. Santopinto in Proceedings of the "Joint ECT*/JLAB Workshop on N* Physics and Nonperturbative QCD", Trento, Italy, May 18-29, 1998, ed. by S. Simula, B. Saghai, N.C. Mukhopadhyay, V.D. Burkert, Few Body Systems, Suppl. 37, 1999.

[40] S. A. Dytman, T. P. Vrana, T. S. H. Lee, piN Newslett, 14, 17(1998).

[41] T. P. Vrana, S. A. Dytman and T. S. H. Lee, submitted to Phys. Rev. C.

[42] M. Giannini, Rep. Prog. Phys. 54, 453(1990).

[43] R.G. Newton, Scattering theory of waves and particles. McGraw-Hill (1969)

[44] R.R. Longacre, J. Dolbeau, Nucl. Phys., B122, 493(1977).

[45] J.M. Blatt, V.F. Weisskopf, Theoretical Nuclear Physics, New York-London (1952).

[46] V. D. Burkert, Czech. Journ. of Phys., Vol.46, 627(1996)

[47] V. Mokeev et al., in Proceedings of the "Joint ECT*/JLAB Workshop on N* Physics and Nonperturbative QCD", Trento, Italy, May 18-29, 1998, ed. by S. Simula, B. Saghai, N.C. Mukhopadhyay, V.D. Burkert, Few Body Systems, Suppl. 11, 1999.

Figure captions

Fig 1. Tree-level diagrams for the $\pi^-\Delta^{++}$ electromagnetic production on proton.

Fig2. ISI and FSI mechanisms.

Fig3. Description of $\pi\Delta$ and ρN elastic scattering amplitudes related to ISI and FSI.

Fig 4. The effective γpN^* vertex (a), the bare γpN^* vertex (b), the dressing vertex correction, containing N^* excitation in $\pi^-\Delta^{++}$ and ρp elastic scattering.

Fig 5a. πN partial wave cross section from [36] decomposed in resonant (dotted lines) background (dashed lines) parts according to procedure described in sect. 3.5. The fit results are shown by solid lines.

Fig 5b. (continued)

Fig 5c. (continued)

Fig 6. The calculated and measured[1] angular distributions for $\gamma p \to \Delta^{++}\pi^-$ reaction assuming negligible contribution for Δ-in- flight term (see text sect. 3). Dashed lines correspond to Born terms alone, while solid lines represent the complete calculation with N^* contribution included.

Fig 7. Decomposition of $\gamma p \to \Delta^{++}\pi^-$ reaction cross section in Born terms (dashed line), N^* terms (dotted line) and interference term (dash-dotted line) contributions. Data are from [1] (squares) and from [7] (circles and triangles).

Fig 8. Total cross section for $\gamma p \to \Delta^{++}\pi^-$ reaction at the photon point. Dashed line represents calculation results with no $\pi N\Delta$ form factor and no ISI and FSI absorptive corrections. Dotted line corresponds to $\pi N\Delta$ strong form factor taken from [32] and no ISI and FSI absorptive corrections. Solid line represents cross section evaluation in the complete model. Data as in Fig. 8.

Fig 9. The calculation with pion Regge trajectory exchange[25]. Solid line represents calculations performed with Born terms evaluated in single pion exchange picture. Dotted line represents the results obtained after substitution of pion exchange by pion Regge trajectory exchange, dashed line corresponds to an additional modification of contact term according to prescription of [25]. Data as in Fig. 8.

Fig 10. The influence of γpN^* vertex dressing effects at the photon point. Our calculations with PDG[13] γpN^* vertices ("dressed") and N^* excitations excluded (solid line) and included (dotted line) in ISI & FSI treatment for Born terms are presented. The calculation results with γpN^* vertices calculated in quark models ("bare" vertices) and with N^* excitation included in ISI & FSI are shown by: dashed line for model [10], dot – dashed line for model [39]. Data as in Fig. 8.

Fig 11. Q^2 dependence of $\gamma_v p \to \Delta^{++}\pi^-$ total virtual photon cross section in comparison with data from [4].

Fig 12. Q^2 dependence of $\gamma p N^*$ vertex dressing effects. Our calculations with $\gamma p N^*$ vertices from [46] ("dressed") and N^* excitations excluded (solid line) and included (dotted line) in ISI & FSI treatment are presented. The calculation results with $\gamma p N^*$ vertices from quark models ("bare" vertices) and with N^* excitation included in ISI & FSI treatment are shown by: dashed line for model [12], dot – dashed line for model [39]. Data from [4].

Table captions

Table 1. List of resonances included in our calculation.

Table 2. List of the resonances predicted by quark models that are weakly coupled to the $N\pi$ channel but should be strongly coupled to the $N\pi\pi$ channels[10].

Table 3. Nucleon resonances contributing in $\pi^-\Delta^{++}$ and $\rho^0 p$ elastic scattering amplitudes.

Table 1:

Resonance, parity	Mass, (MeV)	Width, (MeV)	$\Gamma_{\Delta\pi}$, (%)	$\Gamma_{N\rho}$, (%)	$\frac{\sqrt{\Gamma_{\gamma p}\Gamma_{\Delta\pi}}}{\Gamma_{tot}}$, (%)
$P_{11}(1440)$ +	1430-1470	250-450	20 - 30	< 8	1.06
$D_{13}(1520)$ -	1515-1530	110-135	15 - 25	15 - 25	0.99
$S_{11}(1650)$ -	1640-1680	145-190	1 - 7	4 - 12	0.64
$D_{15}(1675)$ -	1670-1685	140-180	50 - 60	$<$ 1-3	0.70
$F_{15}(1680)$ +	1675-1690	120-140	5 - 15	3 - 15	1.59
$P_{13}(1720)$ +	1650-1750	100-200		70-85	
$S_{31}(1620)$ -	1615-1675	120-180	30 - 60	7 - 25	0.97
$D_{33}(1700)$ -	1670-1770	200-400	30 - 60	30 - 55	3.16
$F_{35}(1905)$ +	1870-1920	280-440	< 25	> 60	0.60
$F_{37}(1950)$ +	1940-1960	290-350	20 -30	< 10	1.50

Table 2:

Resonance, parity	Mass, (MeV)	Γ, (MeV)	$\Gamma_{N\pi\pi}$, (%)	$\Gamma_{\Delta\pi}$, (%)	$\Gamma_{N\rho}$, (%)
P_{13} +	1870	150	14	13	1
P_{11} +	1890	100	34	12	22
P_{13} +	1955	250	63	36	27
F_{15} +	1955	320	41	20	21
F_{35} +	1975	430	100	9	91
P_{33} +	1975	95	99	62	37
P_{13} +	1980	220	76	44	32
P_{11} +	2055	40	12	8	4
P_{13} +	2060	140	33	22	11

Table 3:

Resonance spin	N^* included in resonant part of the amplitudes
1/2	S11(1535), S31(1620), S11(1650), P11(1440), P11(1710), P31(1910)
3/2	P13(1720), P33(1600), P33(1920), D13(1520), D13(1700), D33(1700)
5/2	D15(1675), F15(1680), F35(1905)

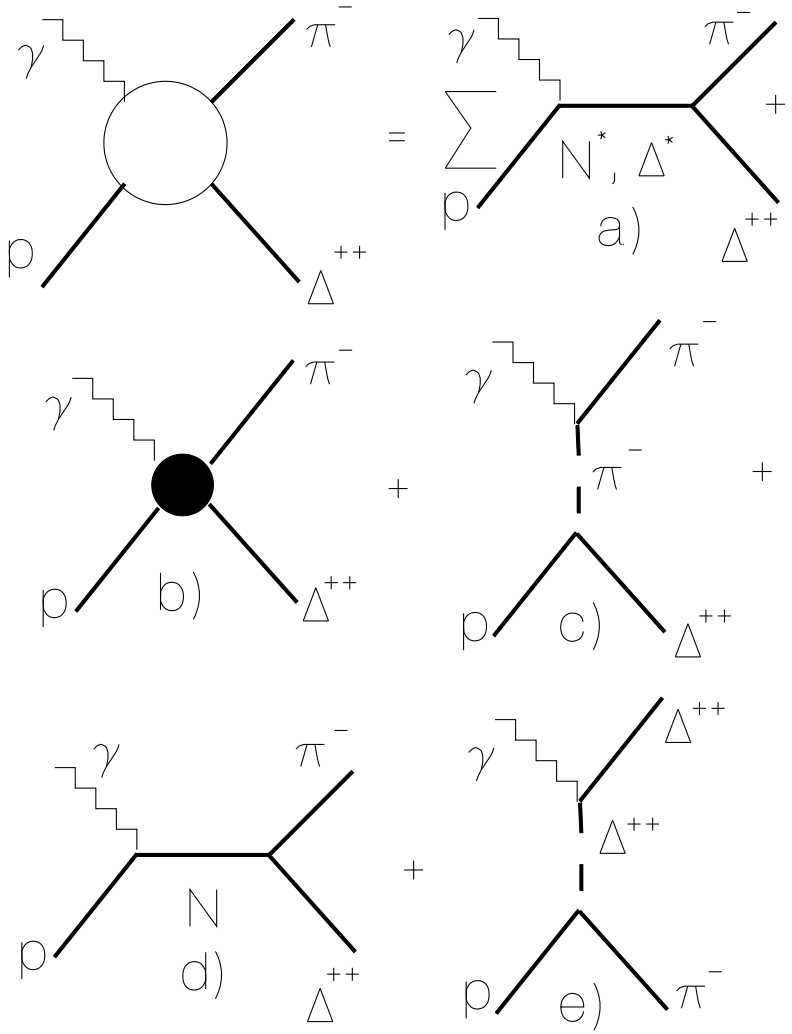

Figure 1

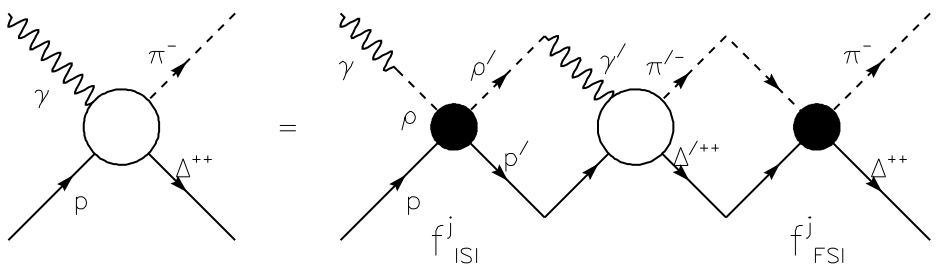

Figure 2

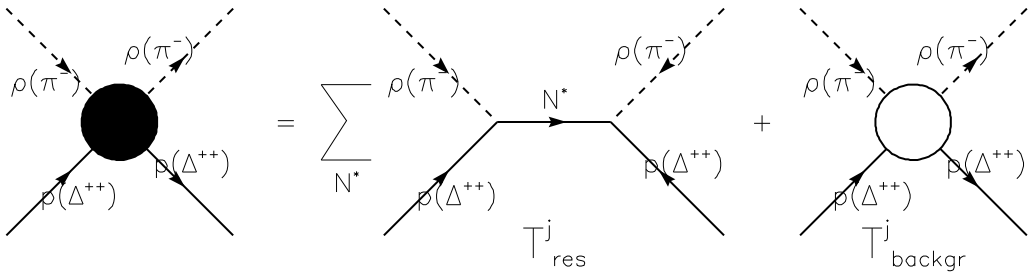

Figure 3

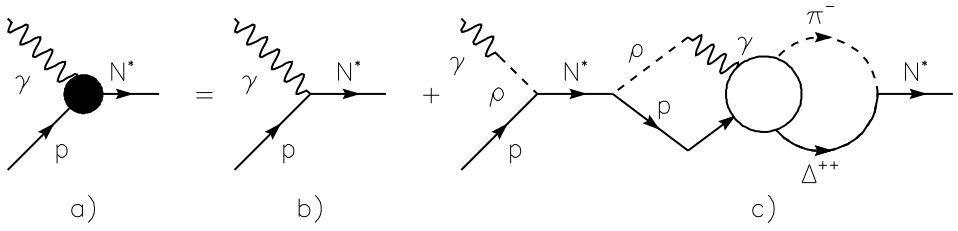

Figure 4

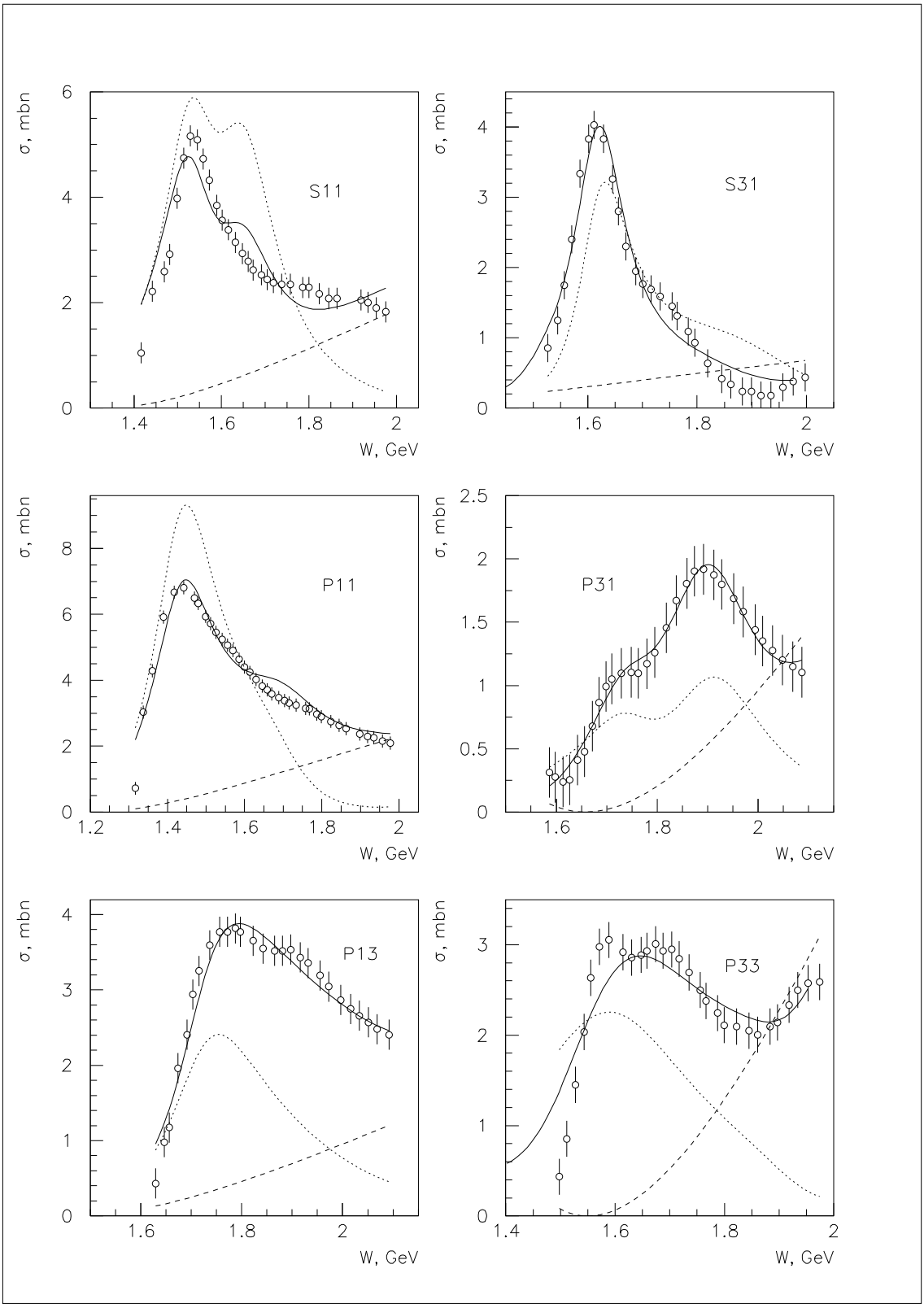
σ, mbn
S11
W, GeV
σ, mbn
S31
W, GeV
σ, mbn
P11
W, GeV
σ, mbn
P31
W, GeV
σ, mbn
P13
W, GeV
σ, mbn
P33
W, GeV

Figure 5a

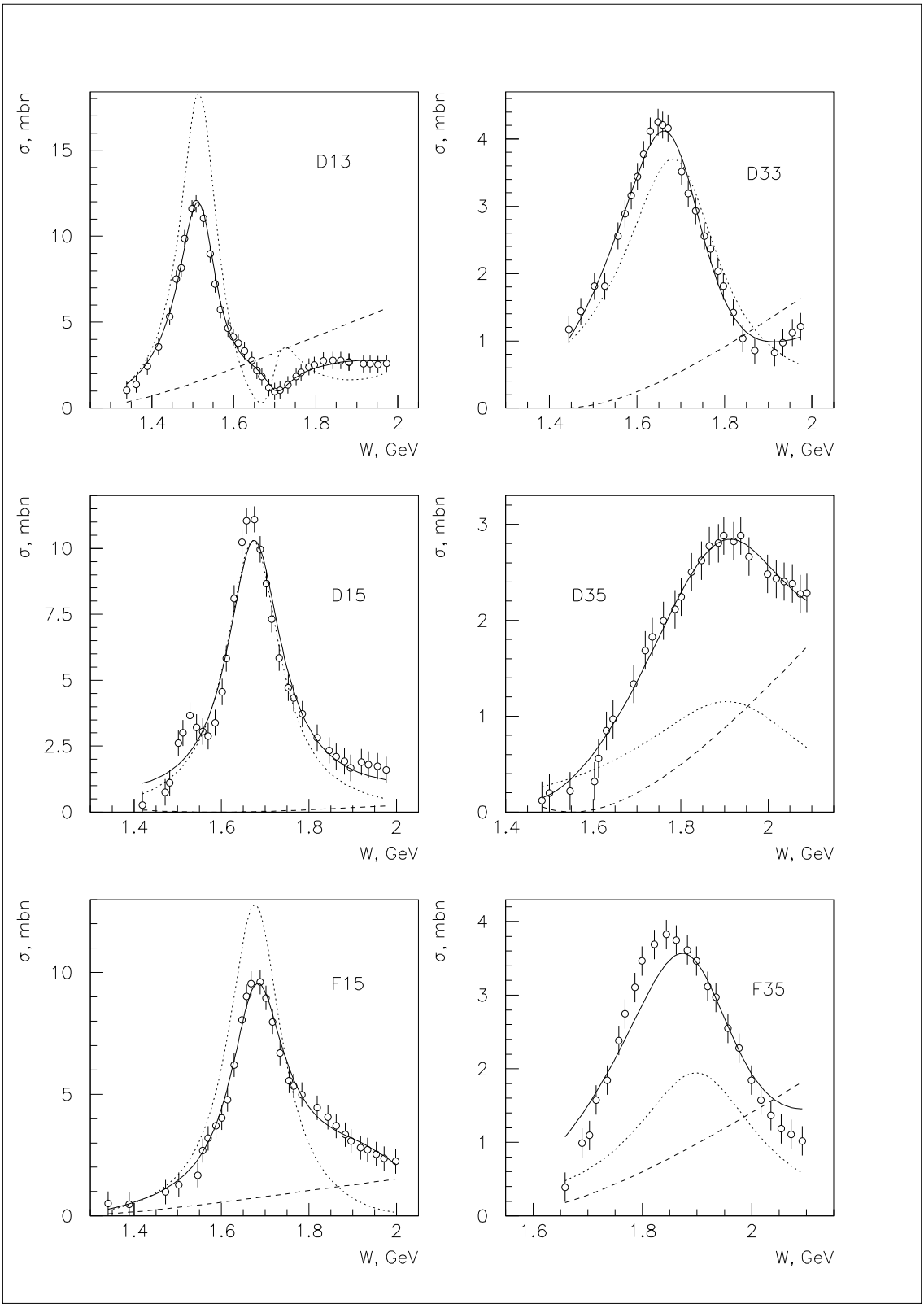
σ, mbn
D13
W, GeV
σ, mbn
D33
W, GeV
σ, mbn
D15
W, GeV
σ, mbn
D35
W, GeV
σ, mbn
F15
W, GeV
σ, mbn
F35
W, GeV

Figure 5b

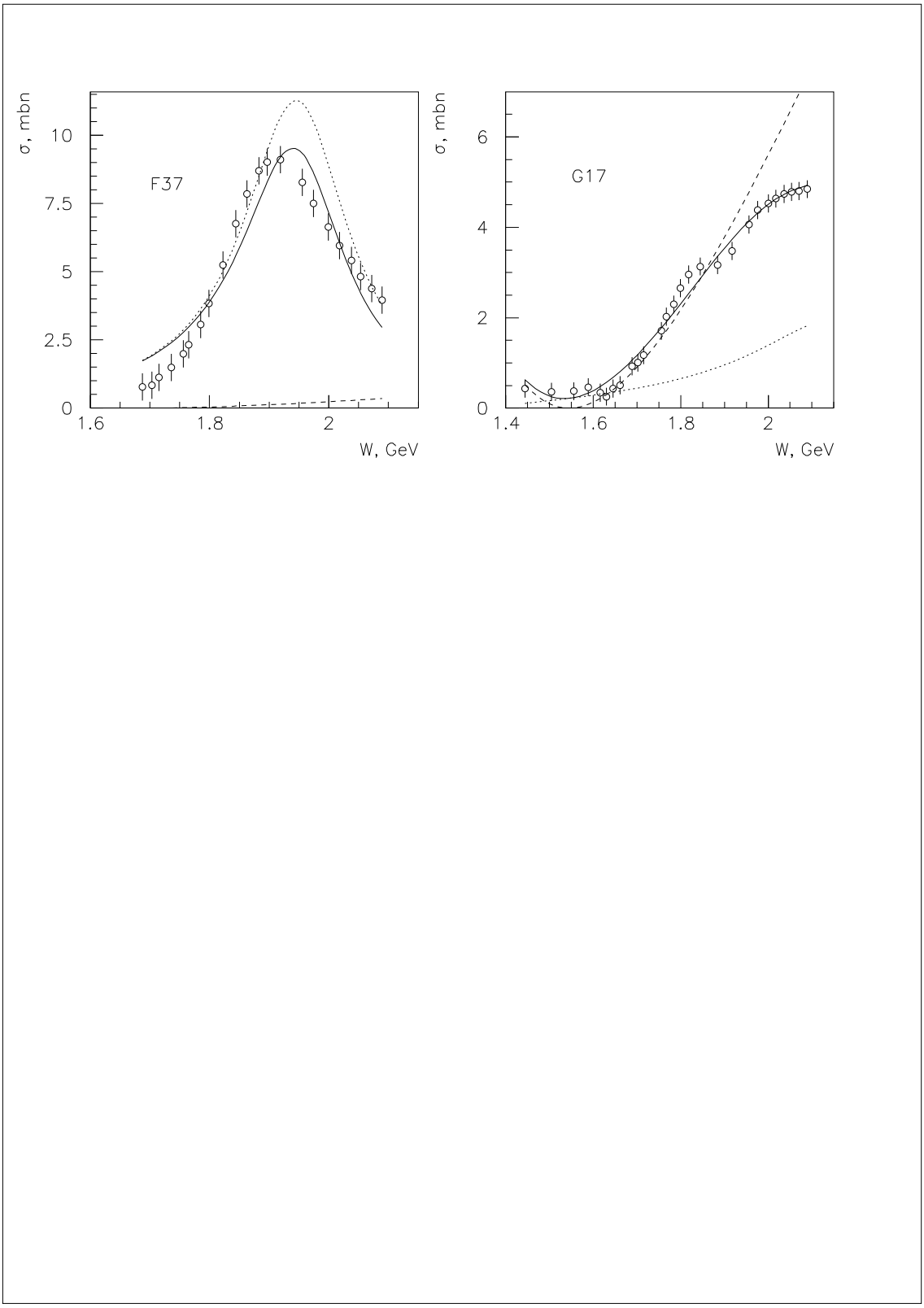

Figure 5c

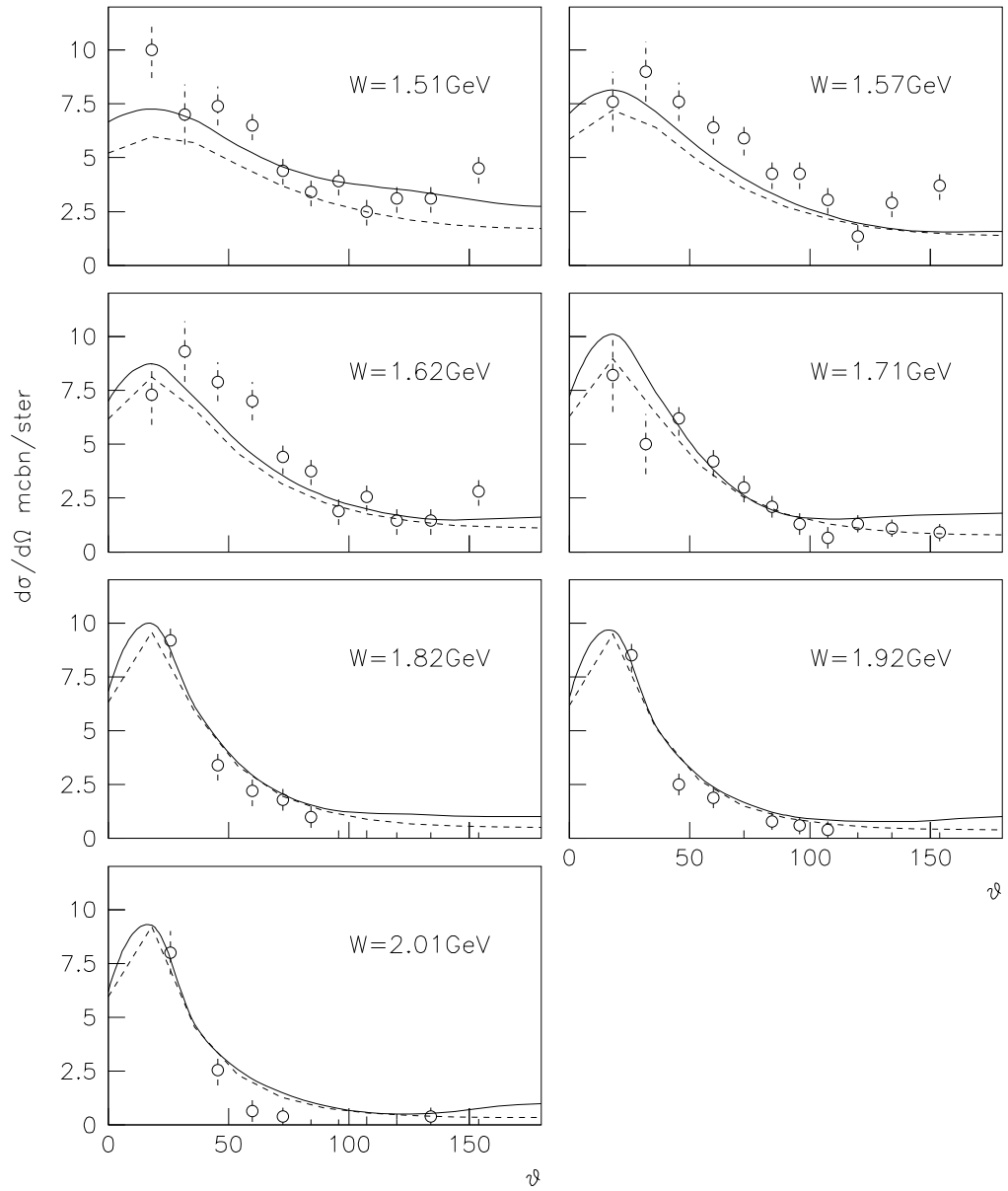
W=1.51GeV
W=1.57GeV
W=1.62GeV
W=1.71GeV
W=1.82GeV
W=1.92GeV
W=2.01GeV
dσ/dΩ mcbn/ster
ϑ
0
2.5
5
7.5
10
50
100
150

Figure 6

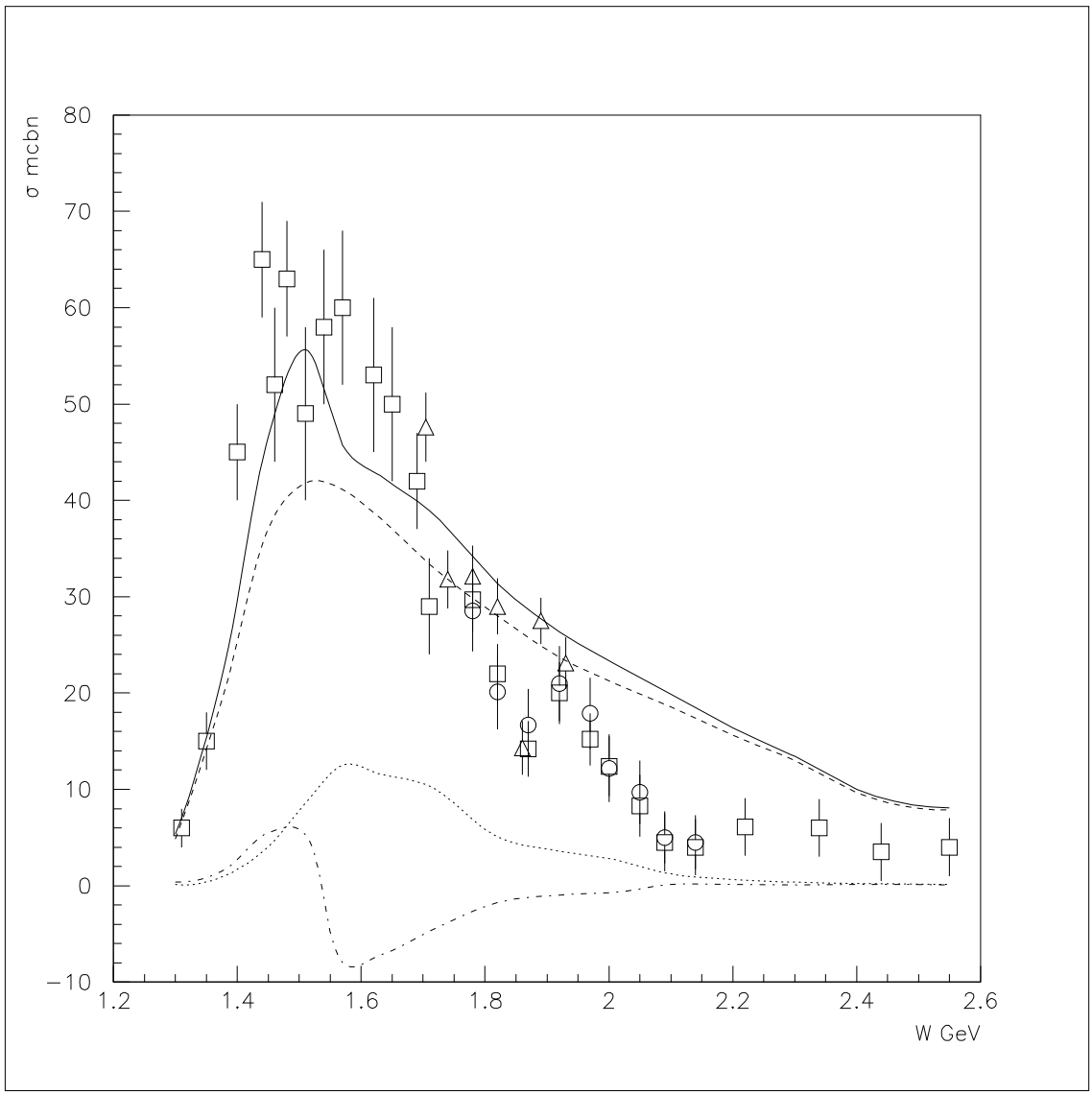

Figure 7

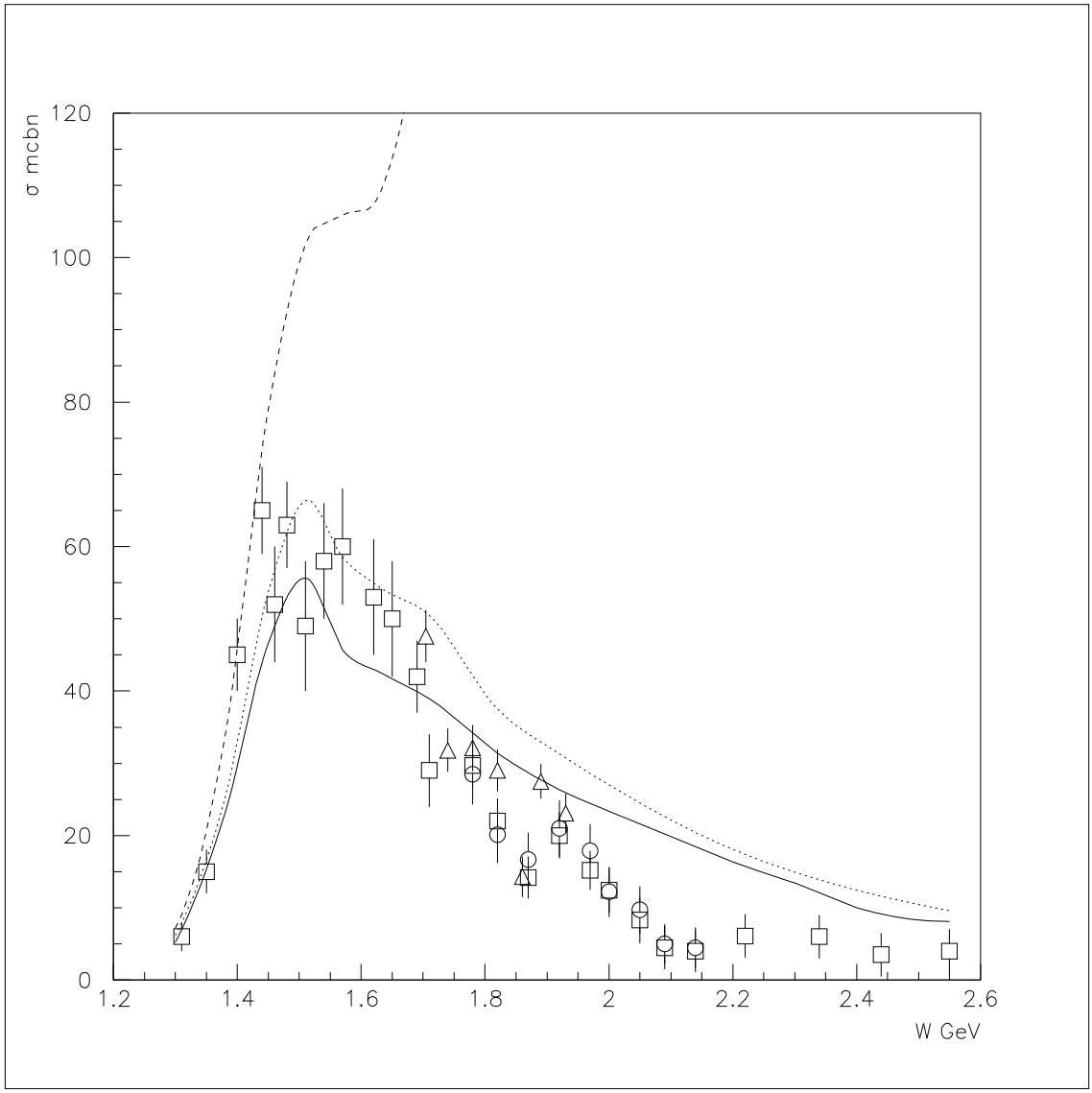

Figure 8

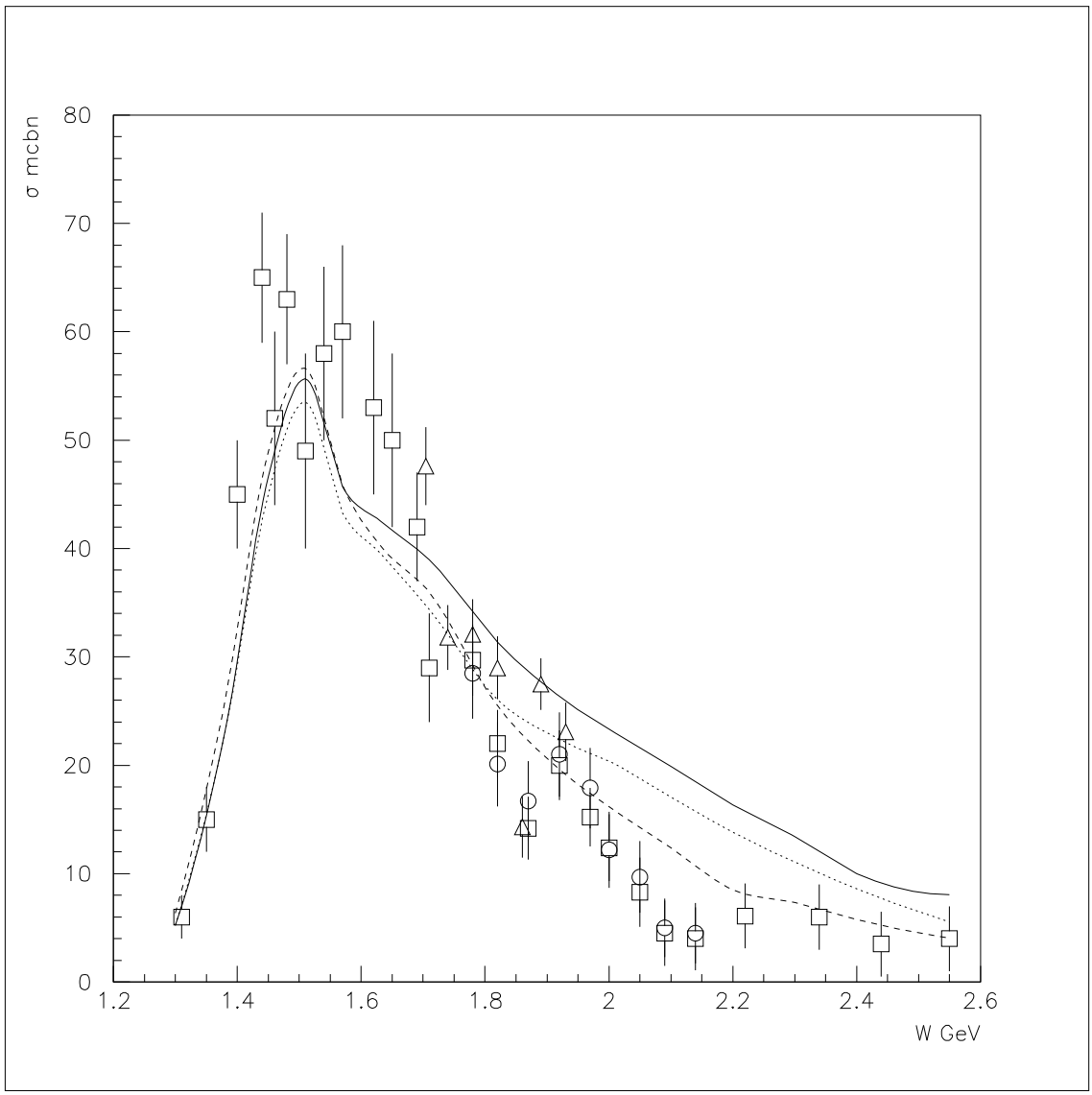

Figure 9

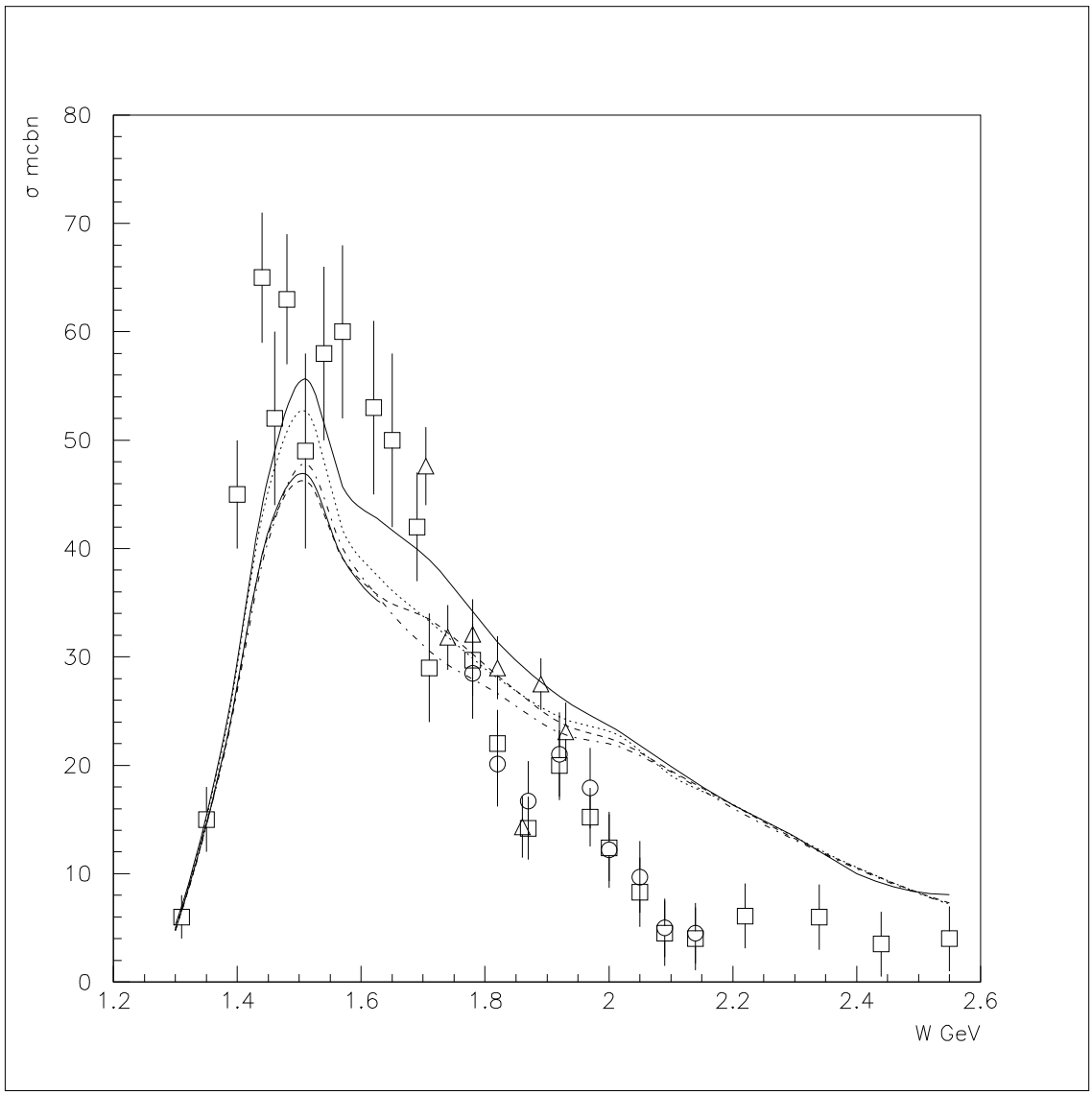

Figure 10

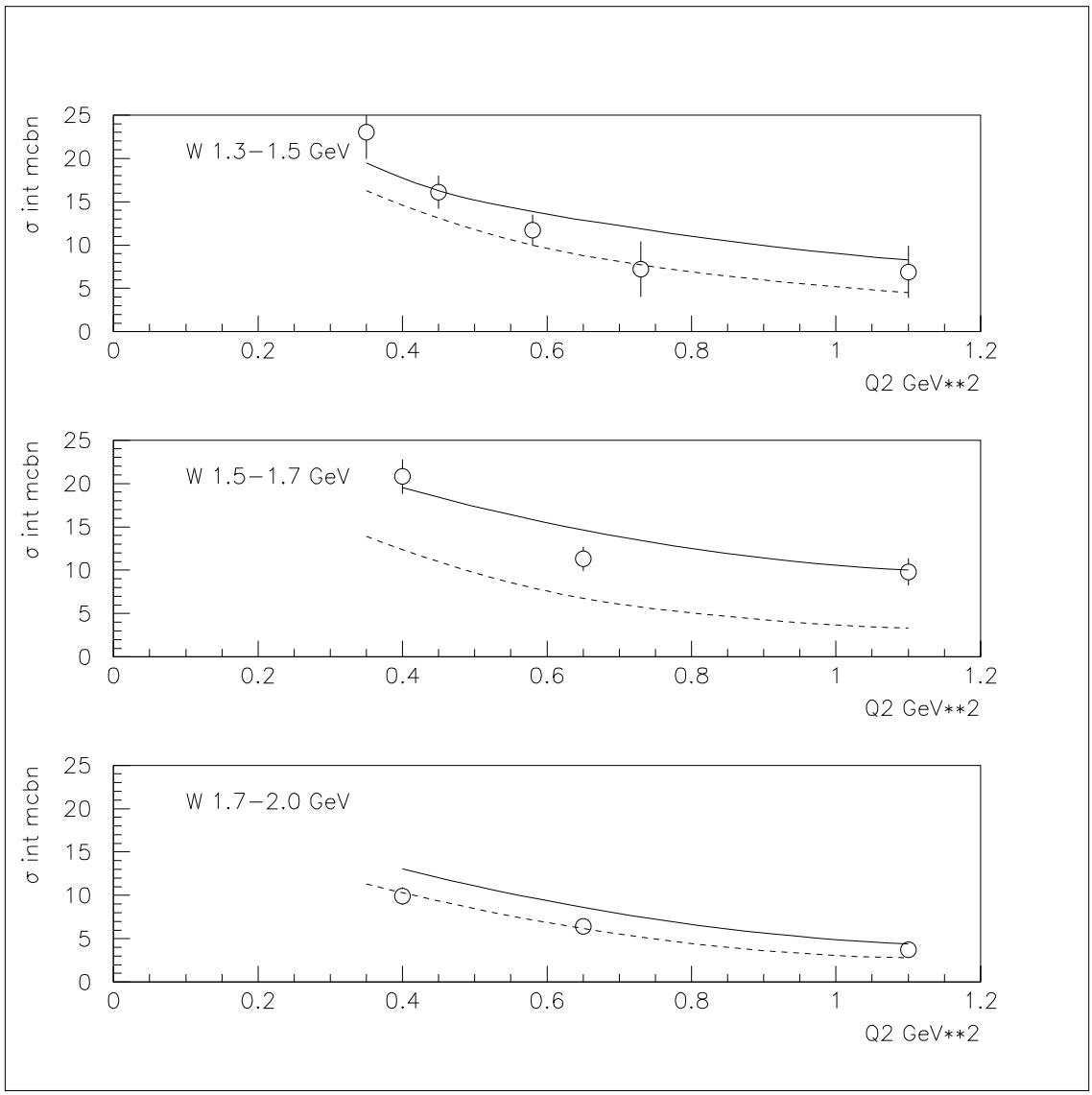
σ int mcbn
W 1.3−1.5 GeV
Q2 GeV**2
σ int mcbn
W 1.5−1.7 GeV
Q2 GeV**2
σ int mcbn
W 1.7−2.0 GeV
Q2 GeV**2

Figure 11

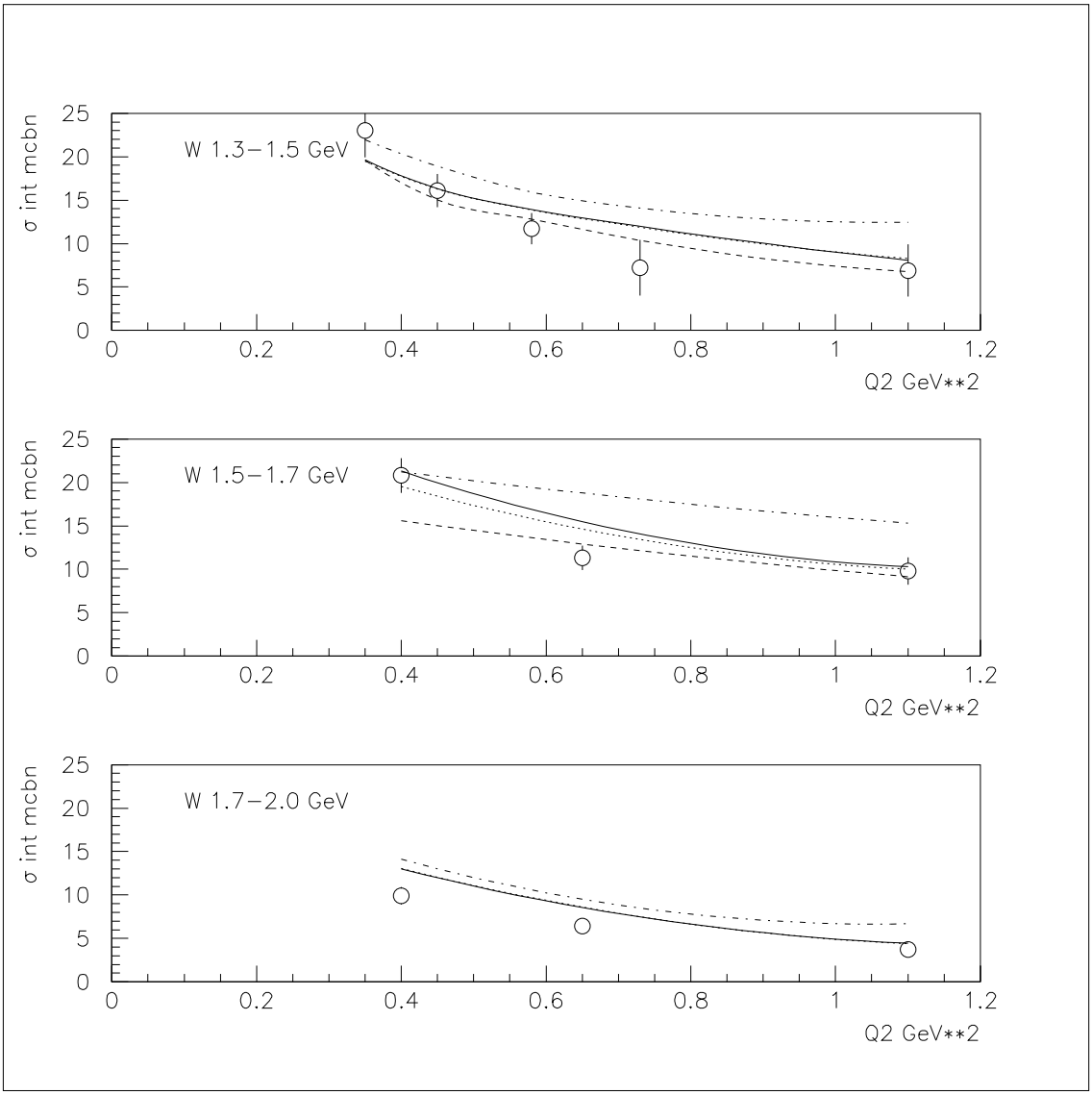
σ int mcbn
W 1.3−1.5 GeV
Q2 GeV**2
σ int mcbn
W 1.5−1.7 GeV
Q2 GeV**2
σ int mcbn
W 1.7−2.0 GeV
Q2 GeV**2

Figure 12